Iberian Variscite mining and consumption: distribution and chronological framework from Pico Centeno (Encinasola, Spain).

Carlos P. Odriozola [a], R. Villalobos-García [b], C.I. Burbidge [c], R. Boaventura [d], A.C. Sousa [d], O. Rodríguez-Ariza [e], R. Parrilla-Giraldez [a], M.I. Prudênçio [c],M.I. Dias [c]

[a] Dpto. de Prehistoria y Arqueología, Universidad de Sevilla. C/ María de Padilla S/N, 41004, Sevilla. Tlf. +34954551415. codriozola@us.es.

[b]Dpto. de Prehistoria, Arqueología, Antropología Social y Ciencias y Técnicas Historiográficas. Universidad de Valladolid. Pz/ del Campus S/N, 47011, Valladolid.

[c] Centro de Ciências e Tecnologias Nucleares, Instituto Superior Técnico, Universidade de Lisboa. E.N. 10 ao km 139,7, 2695-066 Bobadela LRS. Portugal

[d] UNIARQ (Centro de Arqueologia da Universidade de Lisboa). Alameda da Universidade

1600-214 Lisboa. Portugal

[e] Centro Andaluz de Arqueología Ibérica. Universidad de Jaén. Paraje Las Lagunillas s/n, Jaén, España

Abstract:

This paper focuses firstly on dating directly the expoitation of Pico Centeno's mine 2, by means of AMS-radiocarbon dating combined with OSL dating and profiling; and secondly, indirect dating and establishment of an Iberian wide chronological framework through the analysis of well-dated variscite consumption contexts.

The dataset reported in this paper locates the beginning of variscite production at Pico Centeno *c.* 5200 BC, coinciding in time with alpine jade production or Casa Montero iberian flint production.

Variscite consumption is seen as occasional during 5th and 6th millennium BC, and that occurs together with other greenstone. It will be *c.* 3000 BC when variscite use becomes popular and starts its apogee, appearing almost in every Iberian 3rd millennium BC burial, which is the moment when the alpine jade popularity declines.

By the end of this phase, c. 2500 BC, new valuable resources were already in use in the form of signifying items, e.g. asian and african Ivory, Baltic and Sicilian amber or copper-base metallurgy. So the cycle of the variscite starts with the decline jade in the in the 5th – 4th millennium BC, and ends with the appearance of copper, ivory and extra-peninsular amber in the second half of the 3rd millennium BC.

Introduction

Archaeological literature devoted to green body ornaments in Prehistoric Europe has thematically focused, almost with exclusiveness, on the quest for an origin of these artefacts.

Since the early 20th century, the geographical origin of these '*perles du calais*' has moved across continents, from Middle East turquoise mines to European variscite mines, pointing to a French origin firstly at Montebras (Balagny, 1939) or laterly at Pannacé aluminophosphate mines (Forestier et al., 1973a, 1973b; Lheur, 1993; Massé, 1971) and finally to a Spanish origin at Palazuelo de las Cuevas (Arribas et al., 1971, 1970) or Can Tintorer (Alonso et al., 1978; Bosch and Estrada, 1995; Villalba, 2002) variscite mines.

From the 1970s, research devoted to '*calaite*' beads has been oriented to locate and characterise new variscite sources. Since then, new source areas have been discovered at Bragança, Northeast Portugal (Meireles et al., 1987), at the Sarrabus deposit, Sardinia (Marini et al., 1989), the variscite and turquoise outcrops of Punta Corveiro in Spain (Moro et al., 1995), and the Pico Centeno variscite mines, also in Spain (Nocete and Linares, 1999) (fig.1). This focus on source location derives from the belief that the relationship between beads and their geological origin is established principally by comparison of the chemical components of the beads and those of the sources (Edo et al., 1995; Dominguez Bella, 2004; Odriozola, 2014; Odriozola et al., 2010; Querré et al., 2014, 2008). Increased geochemical analyses of sources was paralleled by increase in numbers of analysed beads, and thus in knowledge of the minerals used in the beadmaking, e.g. green mica, steatite, turquoise, talc, chlorite… -see Vázquez Verela. Thus, callaite and variscite can no longer be considered synonyms, and the validity of traditional analysis of variscite[1] flows and consumption patterns has been brought into question: as the number of analysed beads increases it becomes more obvious that prehistoric communities are using almost any available green mineral for beadmaking, from the Neolithic to the Bronze Age.

Present consensus for the geographical origins of European variscite body ornaments points to Palazuelo de las Cuevas (Aliste, Zamora), Can Tintorer (Gavá, Barcelona) and Pico Centeno (Encinasola, Huelva) (Dominguez Bella, 2004; Herbaut and Querré, 2004; Querré et al., 2008, 2014; Odriozola et al., 2010; Odriozola, 2014). However, the chronological span of variscite exploitation is uncertain. The chronology of Palazuelo de las Cuevas and Pico Centeno are uncertain. For Palazuelo de las Cuevas Arribas et al. (1970, 1971) proposed the Arabic period based on the assumption that Zamora was the Arab term for emerald. This proposal was rejected by Virgilio Sevillano (1978) and Campano Lorenzo, et al. (1985), who found TSH pottery and prismatic blanks associated with Las Cercas exploitations, but they did not reject previous Prehistoric interpretations (Sanz Mínguez, et al., 1990). More recent research points

[1] Even today most papers devoted to beads still uses callaite and variscite as synonym.

to a possible Copper Age exploitation in La Mazada (Esparza Arroyo and Larrazabal Galarza, 2000). Can Tintorer has been extensively dated between c. 4500 – 3500 cal. BC –see table 6.

<Figure 1: location of known Iberian variscite sources>

This chronological uncertainty and the tremendous amounts of non-variscite beads motivated the pioneering work of Jiménez Gómez (1995) at the site of Zambujal, where she attempts to chronologically order variscite consumption pattern based on the radiocarbon dates and mineralogical analysis; concluding that in the second half of the 3rd millennium cal. BC the use of variscite become generalised to the detriment of other greenstones used earlier times. Recently Villalobos García (2012) has shown that this generalisation of variscite use for beadmaking during the second half of third millennium BC also happens in the spanish Meseta Norte.

Unfortunately, establishment of variscite flows or consumption patterns has concentrated almost exclusively on source geochemistry and/or consumption, to the detriment of archaeological aspects such as the socioeconomic likelihood for exploitation of the source, and its chronological framework. In consequence, provenance analysis and consumption patterns often pinpoints a geological source that in many cases lacks evidence of exploitation in a relevant timeframe.

Unlike settlements, mines usually do not constitute well-stratified sites, but rather a complex system of use, re-use and re-location of products (Frumkin et al., 2014). Little, if any, datable material survives in direct stratigraphic association with the mined surface. In addition, mines usually experience several exploitation events. Therefore, mine dating tends to be complicated and commonly based on 1. time period-specific mine typology and/or mining technology (tool marks and debris); 2. artefacts typology; and 3. indirectly, throughout the dating of contexts of use of mined materials. Generally, dating of a prehistoric mine based on typology and technology is not a straightforward task. In Iberia this has resulted in chronological frameworks that span Late Prehistory without clear delineation into different late prehistoric periods (Domergue, 1990; Hunt, 2003).

The chronology of exploitation at Pico Centeno is presently controversial. Pérez Macías (2011, 2008) considers the three trench mines found at Pico Centeno to represent Bronze Age and Roman copper exploitation. In addition, Pérez Macías (2008) argued that certain other evidences of possible prehistoric mining at Pico Centeno instead represent soundings made in 1883 by the «Mina de cobre Santo Tomás» (Jubes and Carbonell, 1920). However, a Neolithic-Chalcolithic variscite exploitation has been proposed recently based on Pico Centeno mine 2 (PCM2) typology, typo-technological marks on the surface of the mine, typology of mining tools, and indirectly, throughout the dating of Pico Centeno bead-worked varscite contexts of use (Odriozola et al., 2010; Odriozola, 2014).

This paper pursues a double objective, in the one hand, the dating of Pico Centeno's mine 2 (PCM2), and in the other hand, using the absolute dating recorded for PCM2 in conjunction with radiocarbon dates available for well characterised variscite beads, to generate a time model of variscite exploitation (production) and use (consumption pattern).

Dating of variscite mines is a crucial step in evaluating variscite production, consumption, and its socio-cultural significance. This paper focuses firstly on dating directly the exploitation of PCM2 by means of combined OSL and with AMS-radiocarbon dating of two singular features, an extraction face in which base level we found charcoal, that we thought were related with firesetting, and a pit which we believed correspond to a later exploitation phase by OSL; and secondly, indirectly dating PCM2 through the analysis of well-dated variscite consumption contexts. Both datasets will be the centre of a debate oriented towards the production of a tentative model for variscite production and consumption at an Iberian framework.

PCM2 Direct dating

The outcrop of the Pico Centeno aluminophosphate deposit includes three opencast trench mines which typology resembles that of prehistoric expoitation (Shepherd, 1980; Domergue, 1990; Craddock, 1995; Hunt, 1996, 2003). In addition to early exploitation, indicated by small cavities oriented in the direction of the variscite veins, which represent extraction, and tool marking scars created by mallets and hammerstones, we also detected excavation by metallic picks that could date from roman times to the 20th century 'copper fever' (Pérez Macías, 2008, after Jubes and Carbonell, 1920).

In 2011 we performed an excavation in mine 2 (PCM2), where we conducted 5 test cuts (A-to-E) (fig.2), which recorded features typical of prehistoric activity for this region of Iberia, but also other features suggestive of more recent activity.

<Figure 2>

Prehistoric features may be summarised by an access ramp cut on the rock, a central transit area and an extraction face with small cavities and concave marks leaved by the impact or rounded edged tools, as the found at PCM2 (Odriozola and Villalobos García 2015) –see Craddock (1995) for a detailed view on mining technology. A 2 meters deep pit nearby the access area, which cut the prehistoric facies, and the marks left in the extraction face by metal tools, above those left behind by stone tools, point to an additional non-prehistoric exploitation.

Besides the probability that PCM2 was exploited in recent times, material culture found during excavations, e.g. quartzite cobbles, chisels and picks, points to a prehistoric human activity, most likely related to an early stage of variscite exploitation during Late Prehistory.

The stratigraphy

Pico Centeno, like many other mines in Iberia, exhibits a long history of use, re-use, and re-location of products and debris, resulting in a complex stratigraphy (fig. 3).

<Figure 3: PCM2 stratigraphy>

In PCM2, horizontal units were identified through the stratigraphy. These are interpreted as floor units associated with the mining activities and movement of materials to the exterior of the mine. Cutting these floor units, a deep laterally excavated pit was recorded.

The last floor unit (test cut A SU 9, test cut B SU 11 and test cut C SU 12/13) used before the abandonment of the mine exhibits numerous stone tools such as picks and wedges showing strong use wear, small production debris with concave marks, and charcoal remains adhering to both to extraction faces and the floor. It is believed that the abundance of charcoal in this base level and on the surface results from the use of fire-setting technology (Craddock 1995; Willies 1994; Weisgerber and Willies 2000).

Apparently rapid accumulation of large and medium size rock blocks seals these floor units, indicating filling with debris. Over this debris we recorded several apparently slower, natural, accumulation units, which were sealed by the present use-floor.

In test cut B was encountered a pit that cuts all units almost from the actual surface level. This pit is filled with several horizontal units (SU 21-to-24). Above these units we recorded several anthropic fast deposition and intentional oblique units that fill the pit with large blocks of stone [SU 16-20] (fig. 3 & 4).

Luminescence dating

Five samples were taken for quantitative dating analyses at PCM2: three tubes of sediment (3.8 cm diameter, 15 cm length) and a piece of rock were taken from cut B (units 3, 6, 11, 13 & 18 Figure 4; ITNLUM 696-9, Table 2), and one tube of sediment was taken from cut D (ITNLUM 701, Table 2). Fifteen additional samples were taken for semiquantitative luminescence profiling, using small tubes (2 cm diameter, 5 cm length). Thirteen of these were from the cut B section (Fig 2, Fig 4), and two were taken from the base of the cut C section (Fig 2, Fig 3) (the unexcavated material in cut C was insufficient for a quantitative dating tube).

The East section of test cut B was chosen for OSL dating and profiling since it was the larger conserved stratigraphy (fig. 4) and was expected to include both prehistoric facies and the more modern pit fills. Quantitative samples were taken from the least stony layers, plus one rock to test whether the tailings included material to which fire had been set to facilitate mining. The remaining stratigraphic units were sampled for semiquantitative OSL profiling to test the severity of residual signals in the stonier layers and/or help delimit phases of accumulation. The two additional profiling tubes were taken from the remaining regolith at the base of cut C, close to the 14C sample locations to test chronological relationships between the cuts and between luminescence and 14C results. The sample taken for quantitative analysis from the south section of cut D (ITNLUM 701) was designed to help evaluate the chronological relationship between the fills in cut B and layers of tailings spread around the mine site.

<Figure 4>

<Table 1>

Luminescence and Dosimetric measurements

Luminescence dating measures delayed phosphorescence, obtained from the recombination of electrons and holes in defects of crystalline insulators. Accumulation results from a primary exposure to ionizing irradiation, and recombination of a fraction of those accumulated results from their liberation by secondary irradiation, either by photons (optically stimulated luminescence, OSL) or phonons (thermally stimulated luminescence, TSL) (Burbidge, 2012). The dose of ionizing radiation absorbed by a crystal (Gy) since a liberation event (heating or light exposure), is evaluated by calibrating the OSL or TSL signal obtained from the as-prepared sample material against that produced by controlled irradiations in the laboratory (Burbidge, 2015). Where the accumulated dose of the as-sampled material was produced by ionizing emissions from long-lived radionuclides in a fixed geometry, the dose rate to the crystals in the sample (Gy a^{-1}) may be calculated from parent radionuclide concentrations or direct dose rate measurements of the sample and its environs. From the dose and the dose rate may be calculated the time since the last liberation event (severe heating or light exposure):

Luminescence Age (a) = Absorbed Dose (Gy) / Dose Rate (Gy a^{-1}).

In the present study sampling and analyses for quantitative luminescence dating followed the approach described in Burbidge et al. (2014), based on a combination of instrumental neutron activation analysis (INAA, Dias et al., 2013; Dias and Prudêncio, 2007; Gouveia and Prudêncio, 2000; Prudêncio et al., 2006), high resolution gamma spectrometry (HRGS, Trindade et al., 2013), field gamma spectrometry (FGS; Trindade et al., 2014), water absorption and retention under free drainage, and optically stimulated luminescence (OSL) measurements. Here, FGS was conducted using both Target Nanospec and HPI Rainbow MCAs with 2"x2" NaI probes.

In the laboratory, water content as a fraction of dry (50°C) sample mass was measured as received ("field";W_f), saturated (Ws), and following free drainage for 1 h (0 days), and 1, 2, 4, and 8 days (W_{D0-8}) (Burbidge et al., 2014). One end of each sediment sample (tube) was sealed with tale and the other closed with nylon mesh, the rock was brushed clean of loose material, and weighted (W_f). Inverted tubes and the rock were soaked overnight in deionised water, and weighed after removal of standing water (Ws). Tubes were drained with seals perforated, on an inclined board, the rock was drained on an inclined sieve (W_{D0-8}). Fills rich in weathered pelitic host rock were highly water retentive, the clast-rich mine-waste and the rock less so. Differences between K and Th concentrations estimated by FGS, HRGS and INAA (Table 2) were accounted for using attenuation by W_f (Burbidge et al., 2014) for deeper fills, and representative drained values for samples from drier layers (ITNLUM 696, 701). Since sampling was conducted in late autumn, in days following rain, the time averaged burial values for fill and rock (ITNLUM 696-9) were estimated as the average of each measured in situ water content and that of the driest sample (ITNLUM 701); the maximum value for this was based on its free drainage for 8 days.

The mineralisation associated with precipitation of aluminophosphates to produce Variscite at PCM2 resulted also in the presence of moderately elevated levels of Uranium (Table 2). HRGS was thus conducted for each quantitative dating analysis using 23-31 g of milled material, sealed and equilibriated in polystyrene petri dishes, to test for disequilibrium in the upper U-series. 25 emission lines from ^{40}K and the ^{235}U, ^{238}U and ^{232}Th decay series were mass-normalised and compared with the reference samples GSS1, GSS5, GSR6 used for INAA.

Weighted means over all emissions yielded similar results to INAA (Table 2). U dose rates obtained from (unsealed) FGS measurements, after accounting for in situ water content, were 10%-30% lower than INAA(parent ^{238}U) or Wt Mean HRGS (sealed). The FGS result was considered indicative of minimum ^{222}Rn loss in the field, given the wet conditions, and the FGS U values were preferred for age calculations for the fill and mine-waste samples (ITNLUM 696, 697, 699, 701).

Cosmic dose rate was estimated by averaging values calculated for as-sampled burial depth in regolith, and the height of the adjacent rock, following Prescott and Stephan (1982), and using a fit to the data of Prescott and Hutton (1988) to include the soft component.

<Table 2>

The pelitic host rock produced abundant fine silica, agglomerates of which exhibited slow OSL signal decay, poor recycling and strong recuperation in the SAR-OSL protocol (Murray and Wintle, 2000). Relatively small quantities of 90-160 micron quartz were obtained for quantitative OSL estimation of absorbed dose, by repeated disaggregation, sieving, cleaning with HCl, density separation, HF attack (40%, 40 min), and re-sieving. SAR-OSL measurements were made on 3 Risø DA-15 and DA-20 readers with integrated $^{90}Sr/^{90}Y$ irradiators calibrated relative to the primary ^{60}Co standard of LPSR, CTN metrology laboratory (1, 75±4; 2, 95±3; 3, 111±3, $mGys^{-1}$). The calibration curve used the following doses: 0(As-prepared), 20, 0, 5, 10, 40, 80, 0, 20, 20(IR) sβ; test dose D_T = 10 sβ for ITNLUM 696, 697, 699, 701, with results fitted using a saturating exponential. Initial tests indicated that the quartz grains from sample PCM3 yielded relatively little signal per unit dose (low OSL sensitivity) but that the accumulated dose of the as-prepared sample was relatively large. Thus, the analysis ITNLUM 698 used the following radiation exposures: 0 (As-prepared), 200, 0, 800, 1600, 3200, 6400, 0, 200, 200 (IR); D_T = 50 sβ for, with results fitted using a saturating exponential plus linear function. Preheats were made at 180, 200, 220, 240, 260 and 280 °C/30 s to test for differences in absorbed dose estimates as a function of the relative filling of, and/or transfer of charges between, electron and hole traps during irradiation with the calibration and test doses and their OSL measurement. All measurements using the maximum and minimum preheats were rejected in the analyses ITNLUM 696, 697, 699, 701, since systematic deviations or increased scatter in absorbed dose values were often observed. For the analysis ITNLUM 698, scatter in absorbed dose estimates was great for all preheats, and the test-normalised OSL signal from the as-prepared material did not intercept the calibration curve in two cases (Table 2). For accepted measurements, average recycling ratios ranged from 0.93 to 1.01, and from 0.96 to 1.00 (0.81, ITNLUM 698) after exposure to infrared light. Zero dose response was less than 6% of absorbed dose. OSL sensitivity was relatively low for samples from the pit (Table 2), and for ITNLUM 698 reduced by 50% during the measurement sequence. Signal integrals using the majority of the initial OSL decay, and 'late' background subtraction, were used in all cases: use of the initial signal gradient (second two OSL channels subtracted from the first two channels) resulted in highly dispersed datasets. The weighted mean of the accepted absorbed dose measurements, weighted to inverse variance, appeared representative of the main grouping in the datasets obtained for ITNLUM 696, 697, 699, and 701, and so was used to calculate the central absorbed dose estimates for use in age calculation for all samples. However, the rock (ITNLUM 698) exhibited scatter to very high values of absorbed dose so that the weighted mean is a minimum value only. The results from this sample indicate that the rock was unheated but large finite results were obtained due to poor behaviour within the SAR protocol.

For age estimation, measurements were combined following the approach outlined in Burbidge et al. (2014). Alpha, beta and gamma dose rates from the environment surrounding the sample location were estimated from FGS measurements, after correcting for measurement geometry and the difference between in situ and time averaged water contents. Attenuated environmental dose rates were combined with the self dose rate of a volume of representative size and density, based on the holes excavated for FGS measurement, with values estimated by INAA and HRGS (U from FGS) on material from the adjunct sample taken from those holes, and corrected for time averaged water content estimated from the tube samples. Attenuated dose rates from the environment and adjunct were then combined with similarly estimated values for the samples themselves, which were assumed equal to the adjunct in the case of the tube samples. Dose rates to the etched cores of the grains were calculated from these values, and all combined with calculated cosmic dose rates to estimate total dose rates to the grains measured by luminescence. The absorbed dose from the grains, was divided by the dose rate to estimate time since the event of interest (age), and converted to an estimate of calendar date.

For luminescence profiling (Sanderson et al., 2001), a basic series of preparatory treatments was used, to separate coarse (90–250 µm) 40% HF etched fractions, and measured using a simple multi-stimulation protocol (Rodrigues et al., 2013; Odriozola et al., 2014). The profiling approaches referred to above have calibrated signals from the as-prepared material on an aliquot to aliquot basis, using signals resulting from a single regenerative dose in the quasi-linear region of the sample's dose response. In the present case the as-prepared signals from the profiling samples varied strongly and were often much greater than those produced by the calibration dose. Extrapolation of the quasi-linear calibration dose response would tend to overestimate signal resulting from doses in the range 10-200 Gy, where effects of saturation in the dose response, particularly from quartz, would be expected to be evident. To help account for signal saturation and permit comparison between all results, absorbed dose estimated from the profiling samples were estimated using a common saturating exponential dose response characteristic (DRC) obtained directly from the profiling measurements. This DRC was defined using the average of the standardised (Roberts and Duller, 2004) post-IR OSL responses to 50 sβ (i.e. $D_T I(D=50s\beta)/I_T$), assuming a single saturating exponential dose response, $I = I_\infty(1-\exp(-D/\bar{D}))$, with signal at saturation (I_∞) equal to the average dose of signal saturation ($\bar{D}$), which was found to be 40 Gy, note that D_T in all cases was 10sβ (Burbidge et al., 2006; Burbidge, 2015). Semiquantitative age values were estimated by interpolating total dose rates of the quantitative dating samples.

AMS-Radiocarbon dating

Five radiocarbon measurements were performed using a 1 MV AMS over charcoal sample recovered at the base level of test cut C (unit 12/13).

Chemical preparation of the samples followed standard procedures (Santos Arevalo et al., 2009). Soxhlet extraction was applied using hexane, acetone and ethanol before treating the samples with the Acid–Alkali–Acid cleaning procedure. For the AAA procedure HCl 0.5 M and NaOH 0.1 M were used, and time was carefully controlled to avoid severe losses by dissolution.

Between 7–10 mg of clean and dry charcoal were combusted at 950 °C for 3 h in a vacuum-sealed quartz tube with CuO and Ag powder. Quartz tubes had been previously baked at 950 °C to eliminate possible organic matter. Produced CO_2 was then reduced to graphite by adding excess H_2 and using cobalt as catalyst. The resultant mixture of graphite and cobalt was pressed into aluminium cathodes and kept on vacuum until measurement (Santos Arevalo et al., 2009).

The PCM2 site was very poor in organic materials suitable for radiocarbon dating, and no short lived materials were recovered from excavations: only charcoals from cut C level 12/13 were of sufficient size. AMS-^{14}C dates are reported in conventional radiocarbon years before present in accordance with (Stuiver and Polach, 1977). The results have been calibrated using Calib 7.1 with intcal'13 (Reimer, 2013). Calibrated age is presented in calendar years cal. BC (2 sigma), and also as BP (table 3).

<Table 3>

Anthracological analysis was performed on charcoal fragments, after removal of the samples for AMS-radiocarbon dating. Small size and poor conservation of charcoal samples limited the anthracological determinations, so that in some cases it only allowed determination of angiosperm, and in others to propose a taxon (table 3).

Indirect dating

Ideally evidence should be combined from excavations of several well-dated sites, including beads, pendants or charm-assemblages made from variscite. Unfortunately, accurate identification of bead mineralogy is lacking for most sites in Iberia, where many green minerals other than variscite were used for bead making. In order to realistically define a variscite consumption chronological framework, we need first to identify beads mineralogy.

The mineralogical classification of beads by means of portable analytical devices is not a straightforward task and deserves a full-length paper of its own. However, we have developed a simplified approach for the purpose of helping evaluate bead chronologies.

The mineralogical identifications of beads in this paper (1392 samples from 42 different sites along the Iberian Meseta and Atlantic Façade) are based on the chemical composition measured by an Oxford Instrument XMET-7500 portable x-ray spectrometer with a Rh tube, a silicon drift detector (SDD), and an automatic 5-position filter changer.

Aluminophosphate identification is almost a straightforward task based on Al-to-P atomic ratios. Almost anytime we detect Al-to-P atomic ratio in the compositional range of variscite [[$MPO_4 \cdot 2H_2O$], where M = Al^{3+}, Fe^{3+}, Cr^{3+}, V^{3+} (Larsen, 1942)], from c. 1 to 1.8 (see Odriozola et al., 2010, and Odriozola, 2014), x-ray diffraction confirms that the analysed sample, either geological or beadworked, has variscite as its main crystallographic phase. Thus, here we use the P-to-Al atomic ratio as an indicator to determine variscite as the raw material of beads. Nevertheless, turquoise, crandallite or aheylite may occur separately or as minor crystallographic phases together with variscite (Larsen, 1942). In these cases Al-to-P atomic ratios together with Ca, Cu and Fe values are taken into account to differentiate between minerals.

A much more complicated task is that of differentiating green stones formed by sheet silicates (micas, talc-steatite, chlorite or serpentine). We conservatively classified beads by aluminophosphate, K-aluminosilicates, Mg-aluminosilicates, Mg-silicates and other silicates.

This methodology appears adequate for the purposes of the present work, where the aim is to evaluate whether green beads are worked out of variscite or other greenstone.

Results

Direct dating

The AMS 14C results indicate a palimpsest of organic remains at the base of cut C in the Neolithic (CNA 2144, 2148), Iron Age (CNA 2145), and Mediaeval periods (CNA 2146 2147). The quantitative OSL results from fills indicate accumulation of deposits in cut D and lower cut B in the late 18^{th} – early 19^{th} century AD (ITNLUM 696 697), and in the late 19^{th} century in upper cut B (ITNLUM 699 701) (Table 2). In the present study profiling was conducted only in the laboratory and so was not able to inform the sampling strategy (c.f. Burbidge et al., 2008; Sanderson and Murphy, 2009), but instead was applied in parallel with quantitative dating, to aid interpretation of fill phases and the intensity of accumulation mechanisms that operated during infill of the pit, and to evaluate relationships between sediment layers from around the site that were not amenable to sampling for quantitative analysis (e.g. Odriozola et al., 2014). A frequency plot of the profiling results (f_p, Figure 5) shows how the mineral grains in most of the sampled layers were last exposed to light ca. 7 ka (Neolithic), 0.6 ka (late Mediaeval), and 0.12 ka (Post Mediaeval) These phases correspond with quantitative results obtained by OSL or AMS14C. Many profiling samples, apparently out of stratigraphic sequence, thus appear to contain redeposited material from earlier phases of activity at the site, in which the OSL signal has not been reset: such records are considered useful for interpreting the history of activity at the a site even when removed from their original context, in the same way as survey or recovery of redeposited potsherds (e.g. Deckers et al., 2005; Burbidge et al., 2014).

The OSL profiling results (Figure 5) through the stratigraphy of cut B exhibit two phases of elevated semiquantitative age values, from samples taken in the more stony layers (120-70 cm and 35-25 cm). These are considered indicative of redeposition without (complete) liberation of the trapped charge that is the source of the OSL signal, and hence of rapid redeposition. Quantitative and semiquantitative results from less stony layers associated with them, either immediately below or inter-leaved at approximately the same depth, indicate that their accumulation in their present location corresponds with early and late 19th century infill phases. Results from the first phase (120-70 cm) are scattered, e.g. the difference between the results from the two aliquots measured per sample is large relative to the geometric average value indicated by the trend line in Figure 5, but many results approximate the reproducible (tightly grouped pair) from the sample at the base of cut B (145 cm). This profiling sample, and one of the samples from cut C, yield indications of late Mediaeval accumulation contemporaneous with the youngest AMS14C result from cut C (CNA 2147), and the other profiling sample from cut C gave results consistent with the oldest, Neolithic, AMS 14C results (CNA 2144, 2148).

The late 19th century OSL results are thought to relate to soundings made in 1883 by the Mina de Cobre Santo Tomás, during the 'copper fever'[2] (Pérez Macías, 2008, after Jubes and Carbonell, 1920). However, fills in the lower layers in cut B, and the tailings in cut D unit 3, both relate to an earlier phase of accumulation.

The mixture of charcoals from different periods in the same unit, base level (12/13), indicates phases of repeated use of the cut C space, up to the Mediaeval period, and this is also reflected by semiquantitative OSL results from the bases of cut C and cut B. The space surrounding the void

[2] Copper fever started in Huelva in the mid 19th century.

created by the first miners was last used ca. 600 years ago (bonfires at the border of the pit). PCM2 is in the middle of a copper mining belt of Ossa Morena, exploited since Copper Age and reopened at the end of 19^{th} century with the arrival of British enterprises on the search for copper.

In spite of the calibrated AMS-14C date spam points that PCM2 was probably in use since the transition 6^{th} /5^{th} millennium cal BC (CNA-2141, CNA-2148), which is corroborated by semiquantitative OSL of a small sample of heated sediment, historical occupations are also recorded.

Generally speaking, variscite was exploited for beadmaking during Late Prehistory (Villalba et al., 2001) and during Roman times, for both beadmaking and t*esselae* production (Gutiérrez Pérez et al., 2015). Some weak evidences point to an occasional use during the Bronze Age (Schubart et al., 2004) and in the 18^{th} Century (García-Guinea et al., 2000). It is unlikely that this resource was exploited during 14^{th} century. Pico Centeno is most likely to have been exploited during the Neolithic and Roman periods, when the archaeological record indicates that variscite was used most intensively for beadmaking.

<Figure 5>

Indirect dating

We have built a new dataset of dated sites, together with a bead mineralogical classification (table 4), which creates an ideal framework for the analysis of variscite consumption during Late Prehistory across Iberia. However, we should bear in mind that most of the sites are burials, some of them had long occupations, and accounts for limited number of short-lived 14C dates. If the direct dating of mine contexts has limitations inherent to a continued use of the space, the dating of bead burial contexts (necropolis or settlements) is subject to difficulties of association. Most of the inventoried variscite adornments were collected in early archaeological excavations, without well-defined stratigraphic contexts. However, some trends in bead consumption can be identified.

<Table 4>

If we plot the calibrated dates together with the mineralogical diversity of bead assemblages for each site (fig. 6) we can observe how variscite use could begin in the 5th millennium BC. In figure 6, it can also be appreciated that variscite is not the main mineral used along the 4th millennium BC and that it is during 3rd millennium BC when the use of variscite became generalised, just as has previously been stated for Portuguese Estremadura (Jiménez Gómez, 1995) and the northern Spanish Meseta (Villalobos García, 2012). By the end of 3rd millennium, the use of variscite suddenly stops towards the use of green micas.

<Figure 6>

Discussion

Recorded dates for Pico Centeno's PCM2 variscite mine together with typological and technological criteria show strong evidences of intermittent exploitation during specific periods during Late Prehistory, Iron Age, Medieval Age and Modern Era.

For the Iberian Peninsula, a generalised use of variscite is known for the beginning of Late Prehistory (Villalba et al., 2001) and for roman times (Gutiérrez Pérez et al., 2015); and its use was sporadic in modern times (Garcia-Guinea et al., 2000). It is, therefore, in the light of these data and the historical importance of metal mining at Southwest Iberia, specifically at Encinasola and its surroundings (Pérez Macías, 2008), that 3rd century BC and 9-10th, 14th, 18-19th centuries AD mining activity at Pico Centeno should be most likely related to the exploration of metallic resources rather than variscite itself. We will, thus, focus on the prehistoric use of variscite that is where our main interest rests.

The oldest dates recorded at Pico Centeno for Late Prehistory (5300-5000 and 4900-4700 cal. BC) points to an Early and Middle Neolithic exploitation. However, charcoal radiocarbon dates may be biased towards excessive antiquity by old wood (Schiffer, 1986). The lack of recorded settlements from late 6th millennium BC in the surroundings of Pico Centeno would, to some degree support an old wood effect on the dates. Conversely, a closer look at the available chronologies of Iberian sites that undoubtedly accounts for variscite beads would support an early exploitation of variscite, e.g. Cueva del Moro and Cueva de Chaves (Baldellou et al., 2012) and probably Gruta do Caldeirão (Real,

1992) during 6^{th} millennium cal. BC and Chousa Nova (Dominguez-Bella and Bóveda, 2011), Dolmen de Alberite (Sttip and Tamers, 1996), or Fuentepecina II (Rojo Guerra et al. 1996; Delibes de Castro and Rojo Guerra, 1997) during 5^{th} millennium cal. BC[3].

Coeval in time to earliest variscite use and exploitation, according to PCM2 radiocarbon dates, would be the quarrying and spread of green alpine jade axe around Western Europe (Pétrequin et al., 2006). This phenomenon would be fully coincident in the timing of the overall process of discovery, exploitation and network exchange, to that of variscite being perhaps the scale the biggest difference between both phenomena. Coeval in time to alpine jade axe widest spread and exchange maximum intensification, c. 4500 BC (Pétrequin et al., 2006) (Fig. 6 & Tab. 5).

<Figure 6>

It will be from 4500 cal. BC onwards –mainly in the 4^{th} and first half of 3^{rd} millennia BC- that variscite mining activity increases drastically (Blasco et al., 1992) and the use of variscite become conspicuous in the Iberian Peninsula (Blasco et al., 1997; Bueno Ramírez et al., 2005; Costa et al., 2011; Gonçalves and Reis, 1982; Guitán Rivera and Vázquez-Varela, 1975; Villalobos García, 2012). Therefore, the use of variscite beads become extremely popular, reaching a period of maximum widespread

[3] The later dates should be interpreted with caution, considering the sample types and contexts

and use during the first half of the 3rd millennium BC, while the use of other green stones becomes testimonial (Fig. 7 & Tab. 6).

<Figure 7>

From c. 2500 BC onwards the situation became the opposite, and variscite use starts to decline coinciding with the generalisation of new valuable resources, e.g. Asian and African Ivory (Schuhmacher et al., 2009; Schuhmacher, 2012), Baltic and Sicilian amber (Murillo-Barroso and Martinón-Torres, 2012) or copper-based metallurgy (Murillo-Barroso and Montero Ruiz, 2012).

Concluding remarks

AMS-Radiocarbon and OSL dating of PCM2 dataset reported in this paper show a long-term history of use, from the end of 6th millennium cal. BC Neolithic exploitation of variscite to 19th century AD copper soundings made by Mina de Cobre Santo Tomás.

OSL dating indicates that the fills and tailings currently evident on site accumulated in their present positions in the late 18th and late 19th centuries. AMS-14C dating of apparently *in situ* material set at the rear of the mine excavation indicated a palimsest from the Neolithic, Iron Age and Mediaeval periods. Semiquantiative OSL profiling results, from small samples obtained from stony layers and the remnants of excavated fills not amenable to sampling for fully quantitative OSL analysis, corroborate chronological indications from both quantitative OSL and from AMS-14C. Thus, radiocarbon and OSL provide complementary information on different phases of site usage, linked by luminescence profiling.

The new dataset reported in this paper support a prolonged, intermittent and low intensity mining activity[4]. It locates the beginning of variscite consumption starts coeval in time to the decline jade in the 5th – 4th millennium cal. BC, and the end coinciding with the appearance of other signifying items in the second half of the 3rd millennium BC, e.g. copper, ivory and extra-peninsular amber. Variscite consumption reaches its apogee c. 3000 cal. BC, when appears almost in every Iberian burial (Jiménez Goméz, 1995; Villalobos García, 2012),.

Acknowledgements

The authors acknowledge the Ministerio de Economía y Competitividad (HAR2012-34620) for thr finantial support. Odriozola acknowledges Universidad de Sevilla for a postdoctoral grant. Burbidge acknowledges PTDC/AAC-AMB/121375/2010 for implementation of gamma spectrometry.

8. References

[4] Similar to that of 3rd millennium cal. BC North Iberian copper mining, calculated to be 35 days per annum along 8 centuries (Blas Cortina, 2011)

Acosta, P., 1995. Las culturas del neolítico y calcolítico en Andalucía Occidental. Espacio Tiempo y Forma. Serie Prehistoria y Arqueología 8, 33–80. doi:10.5944/etf+i.8.1995.4720

Alonso, M., Edo, M., Gordo, L., Villalba, M.J., 1978. Explotación minera neolítica en Can Tintorer. Pirenae 13-14, 7–14.

Ambert, P., 2002. Utilisation préhistorique de la technique minière d'abattage au feu dans le district cuprifère de Cabrières (Hérault). Comptes Rendus Palevol 1, 711–716. doi:10.1016/S1631-0683(02)00078-7.

Arribas, A., Galán, E., Martín-Pozas, J.M., Nicolau, J., Salvador, P., 1971. Estudio mineralógico de la variscita de Palazuelo de las Cuevas, Zamora (España). Studia Geologica Salmanticensia 2, 115–132.

Arribas, A., Nicolau, J., Burg, R., 1970. A new ocurrence of variscite in Spain. Lapidary Journal 107, 764.

Balagny, C., 1939. Le mystere de la callais. Societé Archéologique de Nantes 79, 173–216.

Baldellou, V., Utrilla Miranda, P., García-Gazólaz, J., 2012. Variscita de Can Tintorer en el Neolítico Antiguo del Valle Medio del Ebro, In: Borrell, M., Borrell, F., Bosch, J., Clop, X., Molist, M. (Eds.), Actes Xarxes al Neolític. Museu de Gavà, Gavà (Barcelona), pp. 307–314.

Blas Cortina, M.A. de., 2011. Las minas prehistóricas del norte de España en el contexto de la paleominería del cobre del Occidente de Europa. In: Mata-Perelló, J.M., Torró, L., Fuentes, N.M. (Eds.), Actas del V Congreso Internacional sobre minería y Metalurgia Históricas en el Suroeste Europeo. SEDPGYM, MADRID, pp. 101–130.

Blasco, A., Villalba, M.J., Edo i Benaiges, M., 1997. Aspectos sociales del Neolítico Medio catalán. In: Balbín Behrmann, R., Bueno Ramírez, P. (Eds.), II Congreso de Arqueología Peninsular. Neolítico, Calcolítico y Bronce. Fundación Rei Afonso Henriques, Zamora, pp. 89–98.

Blasco, A., Villalba, M.J., Edo, M., 1992. Cronologia del complex miner de Can Tintorer. Aportacions a la periodització del Neolític Mitjà Cátala. In: Estat de La Investigació Sobre El Neolític a Catalunya. 9è Col·loqui International d'Arqueologia de Puigcerdà. Ajuntament de Puigcerdà, Puigcerdà, pp. 215–219.

Boaventura, R., 2011. Chronology of Megalithism in South-Central Portugal. In García Sanjuán, L., Scarre, C., Wheatley, D. (Eds.), Exploring Time and Matter in Prehistoric Monuments: Absolute Chronology and Rare Rocks in European Megaliths. Junta de Andalucía, Sevilla, pp. 159–192.

Borrell, F., Bosch, J., Vicente, O., 2009. Datacions per radiocarboni a les mines neolítiques de la serra de les Ferreres de Gavà. In: Bosch, J., Borrell, F. (Eds.), Intervencions arqueològiques a les Mines de Gavà (sector serra de les Ferreres). Anys 1998-2009. Museu de Gavà, Gavà (Barcelona), pp. 241–246.

Bosch, J., Estrada, A., 1994. El neolític postcardial a les mines prehistòriques de Gavà (Baix Llobregat). Museu de Gavà, Gavà (Barcelona).

Bosch, J., Estrada, A., 1995. La mineria en Gavá (Bajo Llobregat) durante el IV milenio AC. Rubricatum 1, 265–270.

Bueno Ramírez, P., Barroso Bermejo, R., de Balbín Behrmann, R., 2005. Ritual campaniforme, ritual colectivo: la necrópolis de cuevas artificiales del Valle de las Higueras, Huecas, Toledo. Trabajos de prehistoria 62, 67–90.

Burbidge, C.I., 2012. Facets of Luminescence for Dating. Spectroscopy Letters 45, 118–126.

Burbidge, C.I. 2015. A broadly applicable function for describing luminescence dose response. Journal of Applied Physics. Accepted, In Press.

Burbidge, C.I., Duller, G.A.T. and Roberts, H.M. 2006. De determination for young samples using the standardised OSL response of coarse grain quartz. Radiation Measurements 41, 278-288.

Burbidge, C.I., Sanderson, D.C.W. and Fülop, R. 2008. Luminescence dating of ditch fills from the Headland Archaeology Ltd.

excavation of Newry Ring Fort, Northern Ireland, Glasgow, SUERC, University of Glasgow. 91 p.

Burbidge, C.I., Trindade, M.J., Cardoso, G.J.O., Dias, M.I., Oosterbeek, L., Cruz, A., Scarre, C., Cura, P., Caron, L., Prudêncio, M.I., Gouveia, A., Franco, D., Marques, R. 2014. Luminescence dating and associated analyses in transition landscapes of the Alto Ribatejo, Central Portugal. Quaternary Geochronology 20, 65-77.

Burleigh, R., Matthews, K., Ambers, J., 1982. British Museum natural radiocarbon measurements XIV. Radiocarbon 24, 229–261.

Campano Lorenzo, A., Rodriguez Marcos, J.A., Sanz Mínguez, C., 1985. Apuntes para una primera valoración de la explotación y comercio de la variscita en la Meseta Norte. *Anuario del Instituto de Estudios Zamoranos Florián de Ocampo* 13–22.

Cardoso, J.L., 2010. O povoado calcolítico da Penha Verde (Sintra). Estudos Arqueológicos de Oeiras 18, 467–551.

Cardoso, J.L., 2014. Cronología absoluta del fenómeno campaniforme al Norte del estuario del Tajo: implicaciones demográficas y sociales. Trabajos de Prehistoria 71, 56–75.

Cardoso, J.L., Caninas, J.C., 2010. Moita da Ladra (Vila Franca de Xira). Resultados preliminares da escavação integral de um povoado calcolítico muralhado. In: Gonçalves, V.S., Sousa, A.C. (Eds.), Transformação E Mudança No Centro E Sul de Portugal: O 4.o E O 3.o Milénios A.n.e. (Cascais, 2005). Cascais, Cascais, pp. 65–95.

Cardoso, J.L., Carreira, J.R., Ferreira, O. da V., 1996. Novos elementos para o estudo do Neolítico antigo da região de Lisboa. Estudos Arqueológicos de Oeiras 6, 9–26.

Castro Martínez, P.V., Lull, V., Mico, L.R., 1996. Cronología de la Prehistoria Reciente de la Península Ibérica y Baleares (c. 2800-900 cal ANE). Archaeopress, Oxford.

Costa, M.E., García Sanjuán, L., Murillo-Barroso, M., Parrilla Giráldez, R., Wheatley, D.W., 2011. Artefactos elaborados en rocas raras en los contextos funerarios del IV-II milenios cal ANE en el sur de España: Una revisión. Menga 1, 253–294.

Craddock, P.T., 1995. Early metal mining and production. Edinburgh University Press, Edinburgh.

Deckers, K., Sanderson, D.C.W., Spencer, J.Q., 2005. Thermoluminescence screening of non- diagnostic sherds from stream sediments to obtain a preliminary alluvial chronology: an example from Cyprus. Geoarchaeology 20, 67-77.

Delibes de Castro, G., Rojo Guerra, M.Á., 1997. C14 y Secuencia megalítica en la Lora Burgalesa: Acotaciones a la problemática de las dataciones absolutas referentes a yacimientos dolménicos. In: Rodríguez Casal, A.A. (Ed.), O neolitico atlántico e as orixes do megalitismo. Universidad de Santiago de Compostela, Santiago de Compostela, pp. 391–415.

Dias, M.I., Prudêncio, M.I., 2007. Neutron activation analysis of archaeological materials: an overview of the ITN NAA laboratory, Portugal. Archaeometry 49, 383–393.

Dias, M.I., Prudêncio, M.I., Matos, M.A., Rodrigues, A.L., 2013. Tracing the origin of blue and white Chinese Porcelain ordered for the Portuguese market during the Ming dynasty using INAA, Journal of Archaeological Science 40(7) 3046 - 3057. http://dx.doi.org/10.1016/j.jas.2013.03.007

Díaz del Rio, P., Consuegra Rodríguez, S., 2011. Time for action. The chronology of mining events at Casa Montero (Madrid, Spain). In Capote, M., Consuegra, S., Díaz-del-Río, P., Terradas, X. (Eds.), Proceedings of the 2nd International Conference of the UISPP Commission on Flint Mining in Pre- and Protohistoric Times. Archaeopress, Oxford, pp. 221–229.

Díaz del Rio, P., Consuegra Rodríguez, S., Capote, M., Castañeda, N., Criado, C., Vicent García, J.M., Orozco Köhler, T., Terradas Batlle, X., 2008. Estructura, contexto y cronología de la mina de sílex de Casa Montero (Madrid). IV Congreso del Neolítico Peninsular. Museo Arqueológico de Alicante-MARQ, Alicante, pp. 200–207.

Domergue, C., 1990. Les mines de la péninsule Ibérique dans l'Antiquité Romaine, Collection de l'Ecole Française de Rome. École française de Rome, Roma.

Dominguez Bella, S., 2004. Variscite, a prestige mineral in the Neolithic-Aneolithic Europe. Raw material sources and possible distribution routes. Slovak Geological Magazine 10, 147–152.

Dominguez Bella, S., Bóveda, M.J., 2011. Variscita y ámbar en el Neolítico gallego. Análisis arqueométrico del collar del túmulo 1 de Chousa Nova, Silleda (Pontevedra, España). Trabajos de Prehistoria 68, 369–380. doi:10.3989/tp.2011.11075

Edo, M., Blasco, A., Villalba, M.J., Gimeno, D., Fernández Turiel, J.L., Plana, F., 1995. La caracterización de la variscita del complejo minero de Can Tintorer, una experiencia aplicada al conocimiento del sistema de bienes de prestigio durante el neolítico. In: Bernabeu, J., Orozco Köhler, T., Terradas, X. (Eds.), Los Recursos Abióticos En La Prehistoria. Caracterización, Aprovisionamiento E Intercambio. Universitat de Valencia, pp. 83–110.

Esparza Arroyo, A., Larrazabal Galarza, J., 2000. El castro de la Mazada (Zamora): elementos metálicos y contexto peninsular, in: Oliveira Jorge, V. (Ed.), *3º Congresso de Arqueología Peninsular : UTAD, Vila Real, Portugal, Setembro de 1999*. ADECAP, Porto, pp. 433–476.

Fabián García, J.F., 2006. El IV y III milenio AC en el Valle Amblés (Ávila). Junta de Castilla y León, Valladolid.

Fábregas Valcarce, R., Lombera Hermida, A., Rodríguez Rellán, C., 2012. Spain and Portugal: long chisels and perforated axes. Their context and distribution. In: Pétrequin, P., Cassen, S., Errera, M., Klassen, L., Sheridan, A., Pétrequin, A.-M. (Eds.), JADE. Grandes Haches Alpines Du Néolithique Européen. Ve et IVe Millénaires Av. J.-C. Presses Universitaires de Franche-Comté, Besançon, pp. 1108–1135.

Forestier, F.H., Lasnier, B., L'Helgouach, J., 1973a. À propos de la "callaïs", découverte d'un gisement de variscite à Pannecé (Loire-Atlantique), analyse de quelques "perles vertes" néolithiques. Bulletin de la Société Préhistorique Française 70, 173–180.

Forestier, F.H., Lasnier, B., L'Helgouach, J., 1973b. Découverte de minyulite en échantillons spectaculaires, de wavellite et de variscite dans les phtanites siluriens près de Pannecé (Loire-Atlantique). Bulletinde la Société Minéralogique de Cristallographie 96, 67–71.

Frumkin, A., Bar-Matthews, M., Davidovich, U., Langford, B., Porat, R., Ullman, M., Zissu, B., 2014. In-situ dating of ancient quarries and the source of flowstone ("calcite-alabaster") artifacts in the southern Levant. Journal of Archaeological Science 41, 749–758. doi:10.1016/j.jas.2013.09.025

García-Guinea, J., Sapalski, C., Cardenes, V., MLombardero, M., 2000. Mineral inlays in natural stone slabs: techniques, materials and preservation. Construction and Building Materials 14, 365–373.

Gonçalves, V.S., 2002. Quelques questions autor du temps, de l'espace et des symboles mégalithiques du Centre et du Sud Poryugal, in: Origine et Développement Du Mégalithisme de L’ouest de l’Europe (Bougon - 26/30 Octobre 2002). pp. 485–830.

Gonçalves, V.S., 2003. A Anta 2 da Herdade dos Cebolinhos (Reguengos de Monsaraz,Évora): sinopse das intervenções de 1996-97 e duas datações de radiocarbono para a última utilização da Câmara ortostática. Revista Portuguesa de Arqueología 8, 143–188.

Gonçalves, V.S., 2005. Cascais há 5000 mil anos. Tempos, símbolos e espaços da Morte das antigas Sociedades Camponesas. Cámara Municipal de Cascais, Cascais.

Gonc□alves, V.S., 2008. As ocupaçoes pré-históricas das furnas do Poço Velho (Cascais). Cámara Municipal de Cascais, Cascais.

Gonçalves, A.A.H. de B., Reis, M. de L., 1982. Estudo mineralógico de elementos de adorno de cor verde provenientes de estações arqueológicas portuguesas. Portugalia Nova série 2-3, 153–166.

Gouveia, M.A., Prudêncio, M.I., 2000. New data on sixteen reference materials obtained by INAA. Journal of Radioanalitical Nuclear Chemistry. 245, 105–108.

Guitán Rivera, F., Vázquez-Varela, J.M., 1975. Análisis radiográfico de cuentas de calaíta gallegas. Boletín de la Comisión de Monumentos de Lugo 9, 187–188.

Gutiérrez Pérez, J., Villalobos García, R., Odriozola, C.P., 2015. El uso de la variscita en Hispania durante a Época Romana. Análisis de composición de objetos de adorno y teselas de la zona noroccidental de la Meseta Norte. SPAL 24, 165–181.

Herbaut, F., Querré, G., 2004. La parure néolithique en variscite dans le sud de l'Armorique. Bulletin de la Société préhistorique française 101, 497–520. doi:10.3406/bspf.2004.13029

Hunt, M., 1996. Prospección arqueológica de carácter minero y metalúrgico: fuentes y restos. Acontia 2, 19–28.

Hunt, M., 2003. Prehistoric Mining and Metallurgy in South-West Iberian Peninsula. Archaeopres, Oxford.

Jiménez Gómez, M.C., 1995. Zambujal. Los amuletos de las campañas 1964 hasta 1973. In: Sangmeister, E., Jiménez Gómez, M.C. (Eds.), Zambujal: Kupferfunde Aus Den Grabungen 1964 Bis 1973 - Los Amuletos de Las Campañas 1964 Hasta 1973. Philipp von Zabern, Mainz am Rhein, pp. 155–238.

Jubes, E., Carbonell, A., 1920. Estudio geológico-industrial de los yacimientos minerales del término municipal de Encinasola y la Contienda de Moura (Portugal). Boletín Oficial de Minas y Metalúrgia 34–38.

Kunst, M., Lutz, N., 2011. Zambujal (Torres Vedras), Investigações até 2007. Parte 1: Sobre a precisão da cronologia absoluta decorrente das investigações na quarta linha da fortificação. Estudos Arqueologicos de Oeiras 18, 419–466.

Larsen, E.S., 1942. The mineralogy and paragenesis of the variscite nodules from Near Fairfield, Utah part 1. American Mineralogist 27, 281–300.

Lheur, C., 1993. Les minéralisations de l'ancienne carrière de La Floquerie près de Pannecé (Loire-Atlantique). Le Cahier des Micromonteurs 4, 14–21.

Linares Catela, J.A., García Sanjuán, L., 2010. Contribuciones a la cronología absoluta del megalitismo andaluz. Nuevas fechas radiocarbónicas de sitios megalíticos del Andévalo oriental (Huelva). Menga 1, 134–151.

Marini, C., Gimeno, D., Sistu, G., 1989. Le mineralizzazioni a variscite del Sarrabus. Bol. Soc. Geol. It. 108, 357–367.

Massé, R., 1971. Découvert de minyulite, wavellite et variscite dans les phtanites de Pannecé. Bulletin de la Société Sciences naturelles Ouest de la France LXIX, 12–15.

Meireles, C., Ferreira, N., Lourdes Reis, M., 1987. Variscite occurrences in Silurian Formations from Northern Portugal. Comunicações dos Serviços Geológicos de Portugal 73, 21–27.

Moro, M.C., Cembranos Pérez, M.L., Fernández Fernández, A., 1995. Estudio mineralógico de las variscitas y turquesas silúricas de Punta Corveiro (Pontevedra, Españ). Geogaceta 18, 176–179.

Murillo-Barroso, M., Martinón-Torres, M., 2012. Amber Sources and Trade in the Prehistory of the Iberian Peninsula. European Journal of Archaeology 15, 187–216.

Murillo-Barroso, M., Montero Ruiz, I., 2012. Copper Ornaments in the Iberian Chalcolithic: Technology versus Social Demand. Journal of Mediterranean Archaeology 25, 53–73.

Murray, A.S., Wintle, A.G., 2000. Luminescence dating of quartz using an improved single-aliquot regenerative-dose protocol. Radiation Measurements 32, 57–73.

Nocete, F., Linares, J.A., 1999. Las primeras sociedades mineras en Huelva. Alosno. In: Historia de La Provincia de Huelva. Madrid, pp. 49–64.

Odriozola, C.P., 2014. A new approach to determine the geological provenance of variscite artifacts using the P/Al atomic ratios. Archaeological and Anthropological Science 6, 1–22. doi:10.1007/s12520-014-0195-2

Odriozola, C.P. and Villalobos García, R., 2015. La explotación de variscita en el Sinforme de Terena: el complejo minero de Pico Centeno (Encinasola, Huelva). *Trabajos de Prehistoria* 72(2)

Odriozola, C.P., Linares Catela, J.A., Hurtado, V., 2010. Variscite Source and Source Analysis: Testing Assumptions at Pico Centeno (Encinasola, Spain). Journal of Archaeological Science 37, 3146–3157.

Odriozola, C.P., Villalobos García, R., Boaventura, R., Sousa, A.C., Martínez Blanes, J.M., Cardoso, J.L., 2013. Las producciones de adorno personal en rocas verdes del SW peninsular: los casos de Leceia, Moita da Ladra y Penha Verde. Estudos Arqueológicos de Oeiras 20, 605–622.

Odriozola, C.P., Hurtado, V., Dias, M.I., Prudêncio, M.I., 2008. Datación por técnicas luminiscentes de la tumba 3 y el conjunto campaniforme de La Pijotilla (Badajoz, España)./ Luminiscence Dating of Burial 3 and the Bell Beaker pottery from La Pijotilla (Badajoz, Spain). In: VIII Congreso Ibérico de Arqueometría. ACTAS. Instituto de Historia (CSIC), Museo Arqueológico Nacional y SAPaC, pp. 211–225.

Odriozola, C.P., Burbidge, C.I., Dias, M.I., Hurtado, V. 2014. Dating of Las Mesas Copper Age walled enclosure (La Fuente, Spain). Trabajos de Prehistoria, 71, 343-352.

Oliveira, J., 2000. O megalitismo de xisto da Bacia do Sever (Montalvão–Cedillo). In: Gonçalves, V. S. (Ed.), Muitas Antas, Pouca Gente? Instituto Português de Arqueología, Lisboa.

Oliveira, J., 2010. Neolítico e megalitismo na Coudelaria de Alter. In: Transformação E Mudanza No Centro E Sul de Portugal: O 4.o E O 3.o Milénios A.n.e. Cámara Municipal de Cascais, Cascais.

Pavón Soldevila, I., 1994. El mundo funerario de la edad del bronce en la Tierra de Barros: una aproximación desde la bio-arqueología de Las Minitas. Mem. Campaña Urgenc. De 2008–141.

Pérez Macías, J.A., 2008. Recursos minerales de cobre y minería prehistórica en el suroeste de España. Verdolay 11, 9–36.

Pérez Macías, J.A., 2011. Las minas de Encinasola (Huelva). La explotación de un campo filoniano de Ossa Morena. De Re Metallica 16, 1–10.

Pétrequin, P., Cassen, S., Klassen, L., Fábregas Valcarce, R., 2012. La circulation des haches carnacéennes en Europe occidentale. En: Pétrequin, P., Cassen, S., Errera, M., Klassen, L., Sheridan, A., Pétrequin, A.-M. (Eds.), JADE. Grandes haches alpines du Néolithique européen. Ve et IVe millénaires av. J.-C. Presses Universitaires de Franche-Comté, Besançon, pp. 1015–1045.

Pétrequin, P., Errera, M., Martin, A., Fábregas Valcarce, R., Vaquer, J., 2012b. Les haches en jades alpins pendant les Ve et IVe millénaires. L'exemple de l'Espagne et du Portugal dans une perspective Européenne. Rubricatum 5, 213–222.

Pétrequin, P., Errera, M., Petrequin, A.-M., Allard, P., 2006. The Neolithic Quarries of Mont Viso, Piedmont, Italy: Initial Radiocarbon Dates. European Journal of Archaeology 9, 7–30.

Prescott, J.R., Hutton, J.T. 1988. Cosmic-Ray and Gamma-Ray Dosimetry For TL and Electron-Spin- Resonance. Nuclear Tracks and Radiation Measurements 14, 223-227.

Prescott, J.R., Stephan, L.G. 1982. The contribution of cosmic radiation to the environmental dose for thermoluminescent dating. Latitude, altitude and depth dependencies. Council of Europe PACT Journal 6, 17-25.

Prudêncio, M.I., Oliveira, F., Dias, M.I., Sequeira Braga, M.A., Delgado, M., Martins, M. (2006). Raw materials sources used for the manufacture of Roman “Bracarense” ceramics from NW Iberian Peninsula. Clays and Clay Minerals, vol. 54, nº 5, p. 639-651.

Querré, G., Calligaro, T., Domínguez-Bella, S., Cassen, S., 2014. PIXE analyses over a long period: The case of Neolithic variscite jewels from Western Europe (5th–3th millennium BC). Nuclear Instruments and Methods in Physics Research Section B: Beam Interactions with Materials and Atoms 318, 149–156.

Querré, G., Herbault, F., Calligaro, T., 2008. Transport of Neolithic variscites demonstrated by PIXE analysis. X-Ray Spectrometry 37, 116–120.

Real, Fernando, 1992. Estudo Mineralógico de Adornos de Cor Verde Do Neolítico Antigo Da Gruta Do Caldeirão. In João Zilhão *(ed.): Gruta Do Caldeirão O Neolítico Antigo*. Lisboa: Trabalhos de Arqueología 6, Instituto Português do Patrimonio Arquitectónico e Arqueológico. Departamento de Arqueología, 1992. pp. 315–319.

Reimer, P., 2013. IntCal13 and Marine13 Radiocarbon Age Calibration Curves 0–50,000 Years cal BP. Radiocarbon 55, 1869–1887. doi:10.2458/azu_js_rc.55.16947

Roberts, H.M., Duller, G.A.T. 2004. Standardised growth curves for optical dating of sediment using multiple grain aliquots. Radiation Measurements 38, 241-252

Rodrigues, A.L., Burbidge, C.I., Dias, M.I., Rocha, F., Valera, A., Prudêncio, M.I. 2013. Luminescence and mineralogy of profiling samples from negative archaeological features. Mediterranean Archaeology and Archaeometry 13.3, 37-47. ISSN: 1108-9628.

Rojo Guerra, M.Á., Delibes de Castro, G., Edo i Benaiges, M., Fernández Turiel, J.L., 1996. Adornos de calaíta en los ajuares dolménicos de la provincia de Burgos: Apuntes sobre su composición y procedencia. I Congrés del Neolític a la Península Ibérica, Rubricatum 1, 239–250.

Rothenberg, B., Frejeiro, A.B., 1980. Ancient copper mining and smelting at Chinflón (Huelva SW Spain). Br. Mus. Occas. Pap. 20, 41–62.

Sanderson, D.C.W., Bishop, P., Houston, I., Boonsener, M., 2001. Luminescence characterisation of quartz-rich cover sands from NE Thailand. Quaternary Science Reviews 20, 893–900.

Sanderson, D.C.W., Murphy, S. 2009. Using simple portable OSL measurements and laboratory characterisation to help understand complex and heterogeneous sediment sequences for luminescence dating. Quaternary Geochronology 20, 893–900.

Santos Arevalo, F.J., Gómez Martínez, I., Garcia Leon, M., 2009. Radiocarbon Measurement Programme At the Centro Nacional de Aceleradores (CNA). Radiocarbon 883–889.

Sanz Mínguez, C., Campano Lorenzo, A., Rodríguez Marcos, J.A., 1990. Nuevos datos sobre la dispersión de la variscita en la Meseta Norte: las explotaciones de época romana, in: *Primer Congreso de Historia de Zamora. Tomo 2. Prehistoria E Historia Antigua*. Instituto de Estudios Zamoranos Florián de Ocampo, Zamora, pp. 747–764.

Schiffer, M.B., 1986. Radiocarbon dating and the “old wood” problem: The case of the Hohokam chronology. Journal of Archaeological Science 13, 13–30. doi:10.1016/0305-4403(86)90024-5

Schubart, H., Pingel, V., Kunter, M., Liesau von Lettow-Virbeck, C., Pozo, M., Medina, J.A., Casas, J., Tresserras, J.J., Hägg, I., 2004. Studien zu Grab 111 von Fuente Álamo (Almería). Madrider Mitteilungen 45, 57–146.

Schuhmacher, T.X., 2012. El marfil en España desde el Calcolítico al Bronce Antiguo. En: Banerjee, A., López Padilla, J.A., Schuhmacher, T.X. (Eds.), Elfenbeinstudien faszikel 1. Marfiles y elefantes en la península Ibérica y el Mediterráneo Occidental, Iberia Archaeologica. Verlag Philipp von Zabern, Mainz, pp. 45–68.

Schuhmacher, T.X., Cardoso, J.L., Banerjee, A., 2009. Soucing African ivory in Chalcolithic Portugal. Antiquity 83, 983–997.

Senna-Martínez, J.C., Quintã Ventura, J.M., 2000. Os primeiros constructores de megalitos. En: Por Terras de Viriato. Arqueologia Da Região de Viseu. Museo Nacinal de Arqueologia, Viseu.

Shepherd, R., 1980. Prehistoric Mining and Allied industries, Studies in Archaeological Science. Academic Press, London.

Silva, A.M., 2003. Evidence of osteochronditis dissecans in late neolithic/chalcolithic portuguese populations. Dónde Estamos 464–468.

Silva, A.M., Wasterlain, S.N., 2010. A possible case of an ossifying fibroma in a Late Neolithic population from Portugal. Int. J. Osteoarchaeol. 20, 579–585.

Soares, J., 2010. Dólmen da Pedra Branca. Datas radiométricas. Musa Mus. Arqueol. E Outros Patrimónios 3, 71–82.

Soares, J., SIlva, C.., 2010. Anta Grande do Zambujeiro - arquitectura e poder. Intervenção arqueológica do MAEDS, 1985-87. Musa Mus. Arqueol. E Outros Patrimónios 3, 83–129.

Sousa, A.C., 2010. Penedos e muralhas. A leitura possível das fortificaçoes do Penedo do Lexim, in: Gonc□alves, V.S., Sousa, A.C. (Eds.), Transformação E Mudanza No Centro E Sul de POrtugal: O 4.o E O 3.o Milénios A.n.e. Cámara Municipal de Cascais, Cascais.

Sttip, J.J., Tamers, M.A., 1996. Dataciones absolutas, in: Ramos Muñoz, J., Giles Pacheco, F. (Eds.), El Dolmen de Alberite (Villamartín). Aportaciones a Las Formas Económicas Y Sociales de Las Comunidades Neolíticas En El Noroeste de Cádiz. Servicio de publicaciones de la Universidad de Cádiz, Salamanca, pp. 179–186.

Stuiver, M., Polach, H.A., 1977. Discussion: reporting 14C data. Radiocarbon 19, 255–363.

Sousa, A.C., 2010. O Penedo do Lexim e a sequência do Neolítico Final e Calcolítico da Península de Lisboa. (http://repositorio.ul.pt/handle/10451/3480, accesed 2015-02-05 13:39:10).

Tarriño, A., Lobo, P.J., García-Rojas, M., Elorrieta, I., Orue, I., Bento-Calvo, A., Karampanglidis, T., 2011. Introducción al estudio de las minas neolíticas de sílex de la Sierra de Araico (Condado de Treviño):

campaña de excavación del 2011. Estudios de Arqueología Alavesa. 27, 4-81.

Trindade, M.J., Prudêncio, M.I., Burbidge, C.I., Dias, M.I., Cardoso, G., Marques, R., Rocha, F. 2013. Distribution of naturally occurring radionuclides (K, Th and U) in weathered rocks of various lithological types from the uranium bearing region of Fornos de Algodres, Portugal. Mediterranean Archaeology and Archaeometry 13.3, 71-79. ISSN: 1108-9628.

Trindade, M.J., Prudêncio, M.I., Burbidge, C.I., Dias, M.I., Cardoso, G., Marques, R., Rocha, F. 2014. Study of an aplite dyke from the Beira uraniferous province in Fornos de Algodres area (Central Portugal): trace elements distribution and evaluation of natural radioactivity. Applied Geochemistry. 44, 111-120.

Valera, A.C., Silva, A.M., Márquez Romero, J.E., 2014. La temporalidad del recinto de fosos de Perdigões: cronología absoluta de estructuras y prácticas sociales. Spal 23, 11–26. doi:10.12795/spal.2014i23.01

Vaquer, J., Martín, A., Pétrequin, P., Pétrequin, A.-M., Errera, M., 2012. Les haches alpines dans les sépultures du Néolithique moyen pyrénéen: importations et influences. In: Pétrequin, P., Cassen, S., Errera, M., Klassen, L., Sheridan, A., Pétrequin, A.-M. (Eds.), JADE. Grandes Haches Alpines Du Néolithique Européen. Ve et IVe

Millénaires Av. J.-C. Presses Universitaires de Franche-Comté, Besançon, pp. 872–917.

Vázquez Varela, J.M., 1975. Cuentas de "calaita" en la Península Ibérica: datos para la revisión del problema. *Gallaecia* 1, pp. 25–30.

Villalba, M.J., 2002. Le gîte de variscite de Can Tintorer: production, transformation et circulation du minéral vert, in: Guilaine, J. (Ed.), Matériaux, Productions, Circulations Du Neolithique À l'Age Du Bronze. Séminaire Du Collège Du France. Errance, Paris, pp. 115–130.

Villalba, M.J., Edo i Benaiges, M., Blasco, A., 2001. La callaïs en Europe du Sud-Ouest. État de la question, in: Le Roux, C.-T. (Ed.), Du monde des chasseurs à celui des métallurgistes, Revue Archéologique de l'Ouest. Suppléments. Université Rennes I, pp. 267–276.

Villalobos García, R., 2012. Adornos exóticos en los sepulcros tardoneolíticos de la Submeseta Norte Española. El ejemplo de Las Tuerces como nodo de una red descentralizada de intercambios. In: Actes Xarxes al Neolític. Museu de Gavà, Gavà (Barcelona), pp. 265–271.

Villalobos García, R., 2014. The megalithic tombs of the Spanish Northern Meseta. Material, political and ideological tie between the Neolithic people and their territory. In: Colloque Internationel Fonctions, Utilisations et Représentations de L'espace Dans Les Sépultures Monumentales Du Néolithique Européen. Préhistoires

Méditerranéennes, s4. Maison Méditerranéenne Des Sciences de L'homme. CNRS, Université de Provence, Aix-en-Provence.

Virgilio Sevillano, F., 1978. *Testimonio arqueológico de la provincia de Zamora*. Instituto de Estudios Zamoranos "Florian do Campo," Zamora.

Waterman, A.J., 2012. Marked in life and death: identifying biological markers of social differentiation in late prehistoric Portugal.

Weisgerber, G., Willies, L., 2000. The use of fire in prehistoric and ancient mining: firesetting. Paléorient 131–149.

Willies, L., 1994. Firesetting technology. Bulletin of the Peak District Mines Historical Society 12.

Whittle, A.W.R., Healy, F.M.A., Bayliss, A., 2011. Gathering time: dating the early Neolithic enclosures of southern Britain and Ireland. Oxbow Books.

Caption to figures

Figure 1: location of known Iberian variscite sources. Pico Centeno coordinates: Lon: 22º51'29''; Lat:5º13'15'' (ETRS89).

Figure 2: test cut position and 3D model

Figure 3: a) PCM2 planimetry and cuts A, B and C North profiles and cut

B East profile stratigraphies; b) Harris matrix of Cut B (software matrix harris composer).

Figure 4: a) cut B East profile stratigraphy and b) cut D North profile stratigraphy, with detailed quantitative OSL sample position (big dots) and semiquantitative OSL profiling (small dots).

Figure 5: Chronological results from PCM2; note log time axis

Figure 6: radiocarbon calibrated age sum probability plot and pie chart mineralogical identifications for studied sites.

Figure 7: calibrated data for european flilnt, jade, variscite and copper mining. With detail calibrated multisample probability plot of PCM2 radiocarbon dates and sum probabiolity plot flint, jade, variscite and copper european radiocarbon dates.

Tables:

Table 1. Brief description of the OSL dating sampled units.

Table 2a: Luminescence dating measurements: radionuclide concentrations and water content estimates.

Table 2b: Luminescence dating measurements: summary dose rate, dose, and calendar date estimates.

Table 3. Results of AMS-radiocarbon dating and anthracological analysis of sampled charcoals from PCM2.

Table 4. Results of AMS-radiocarbon dating and anthracological analysis of sampled charcoals from PCM2.

Table 5. European mining resources available radiocarbon dates

Table 6: Studied sites available radiocarbon dates

Figure1
Click here to download high resolution image

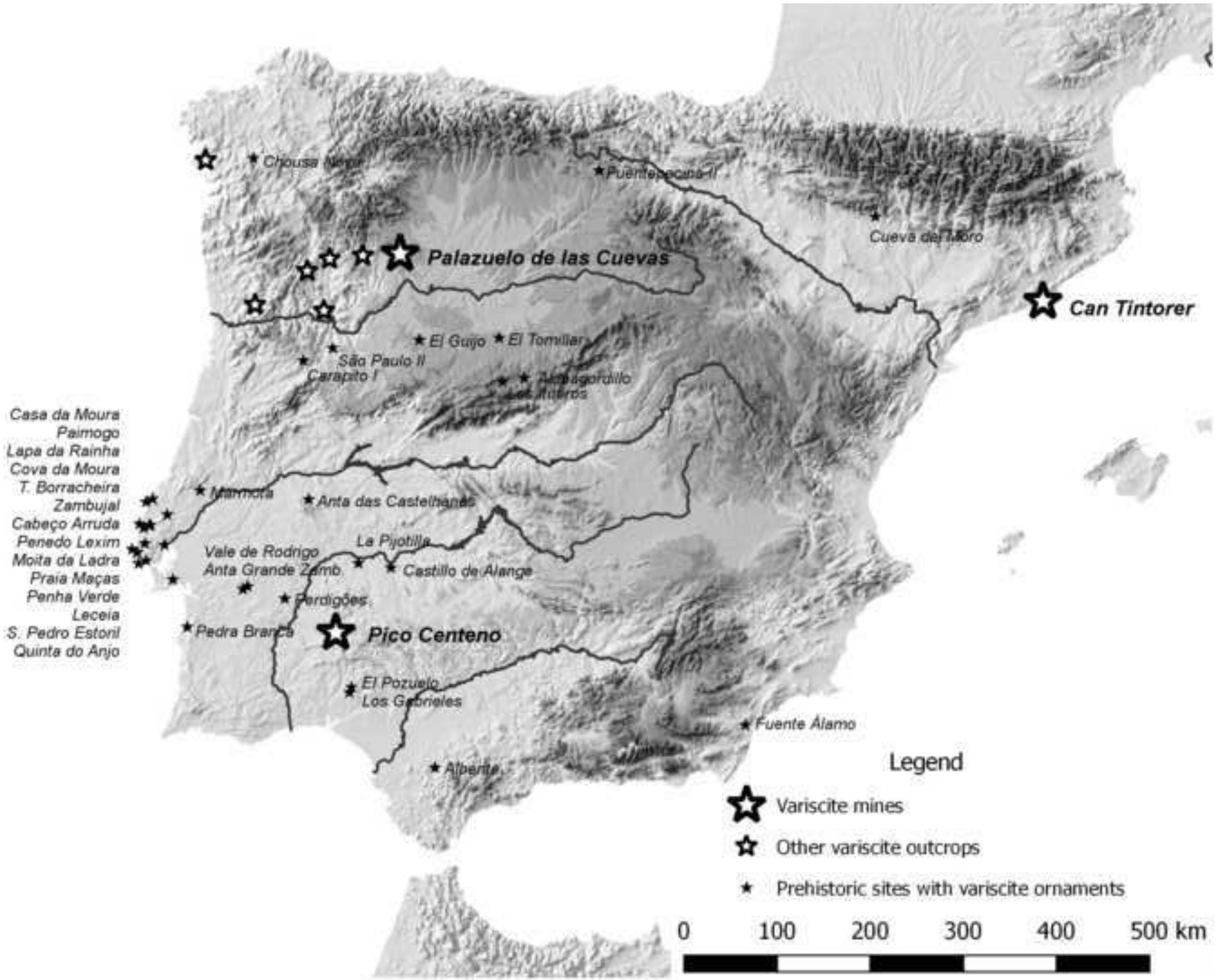

Figure2
Click here to download high resolution image

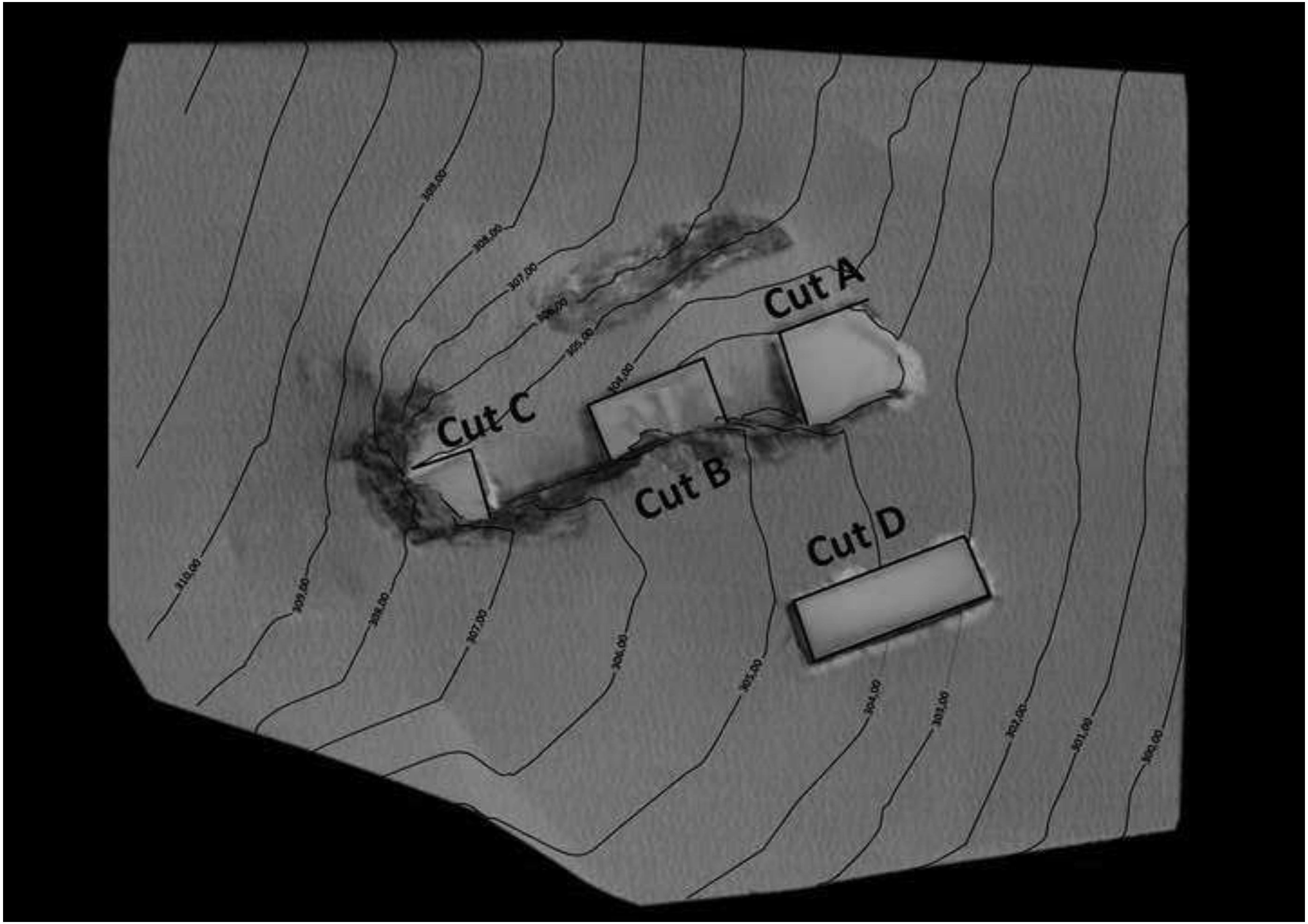

Figure3a

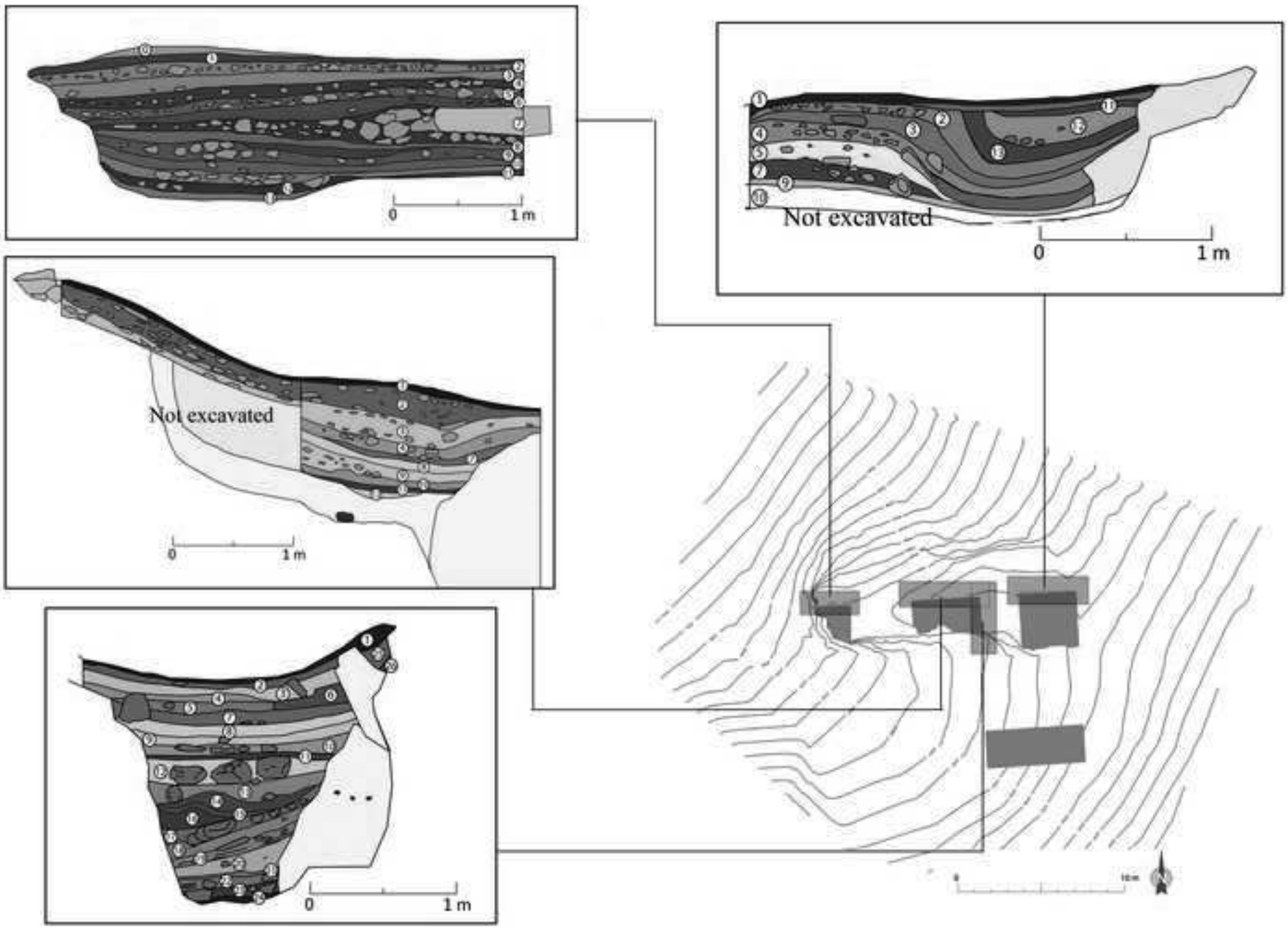

Figure3b
Click here to download Figure: Fig.3b.eps

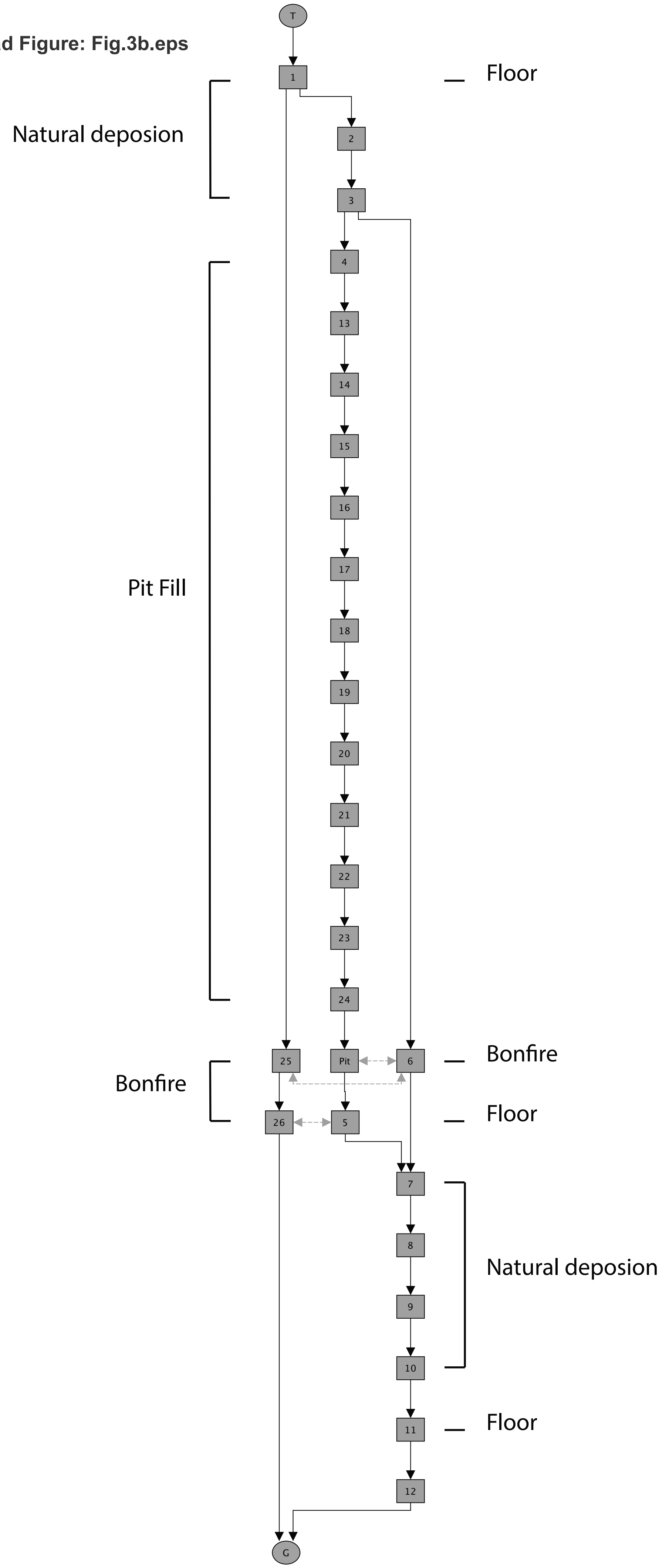

Figure4a
Click here to download high resolution image

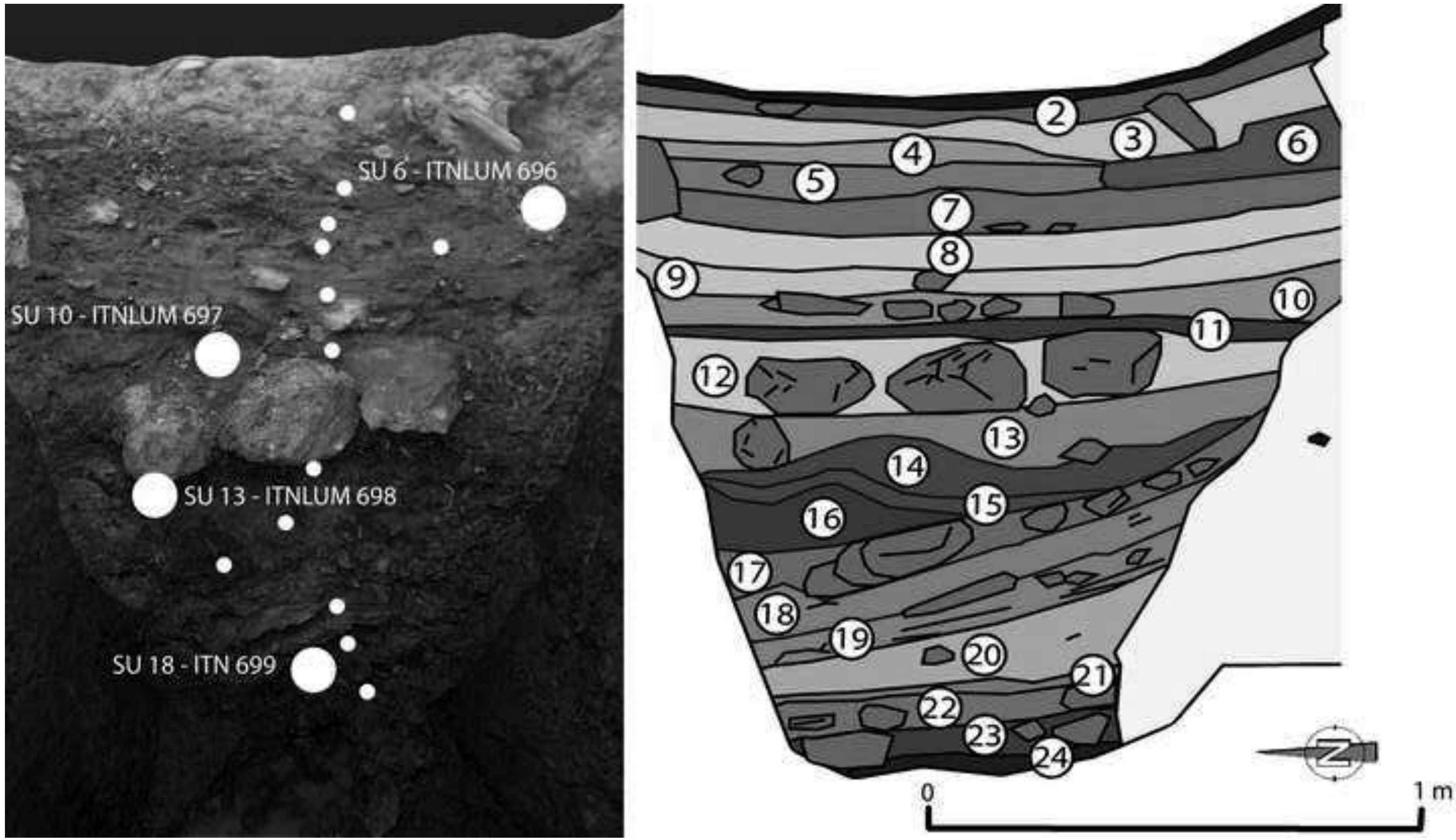

Figure4b

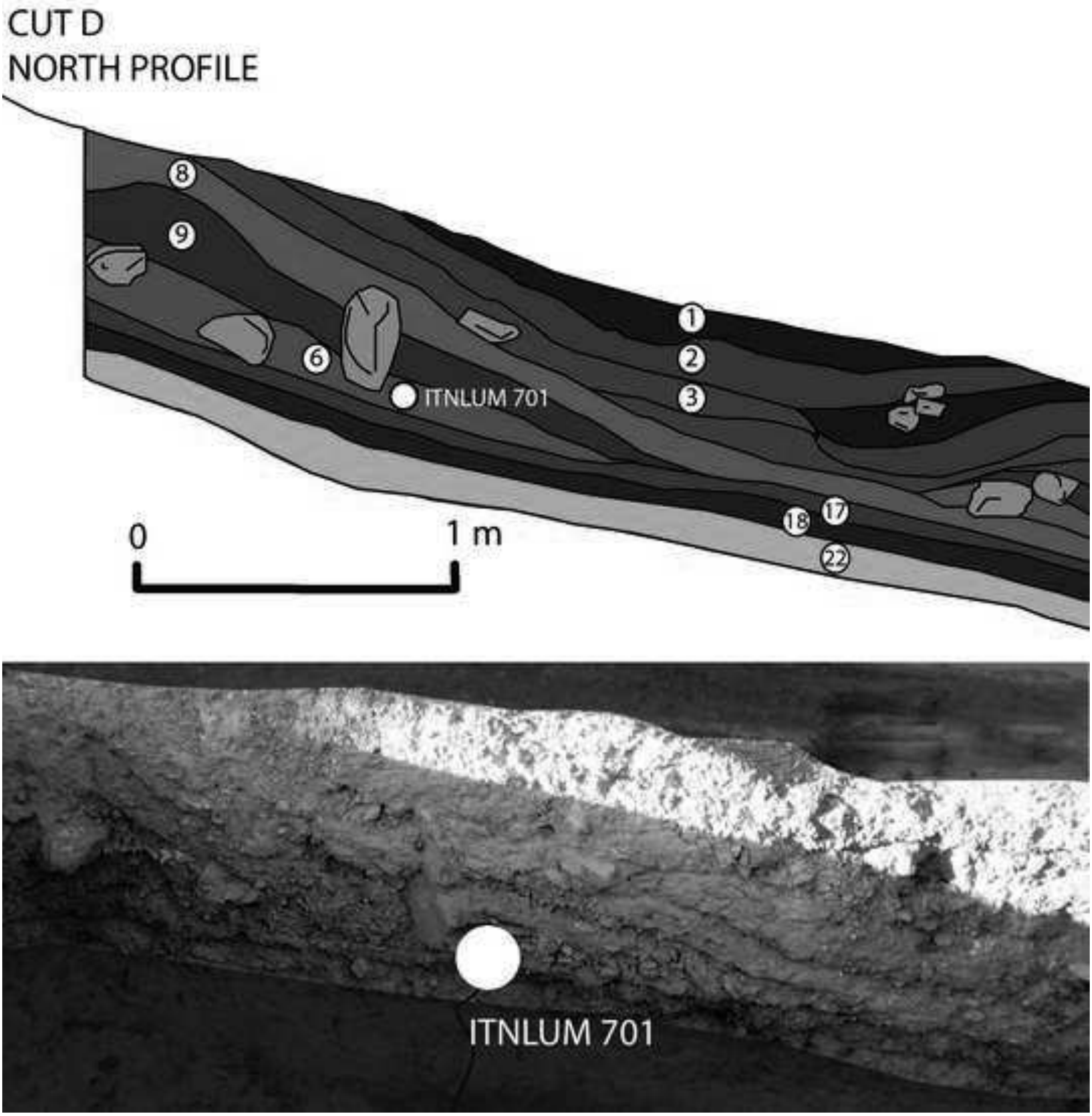

Figure5
Click here to download high resolution image

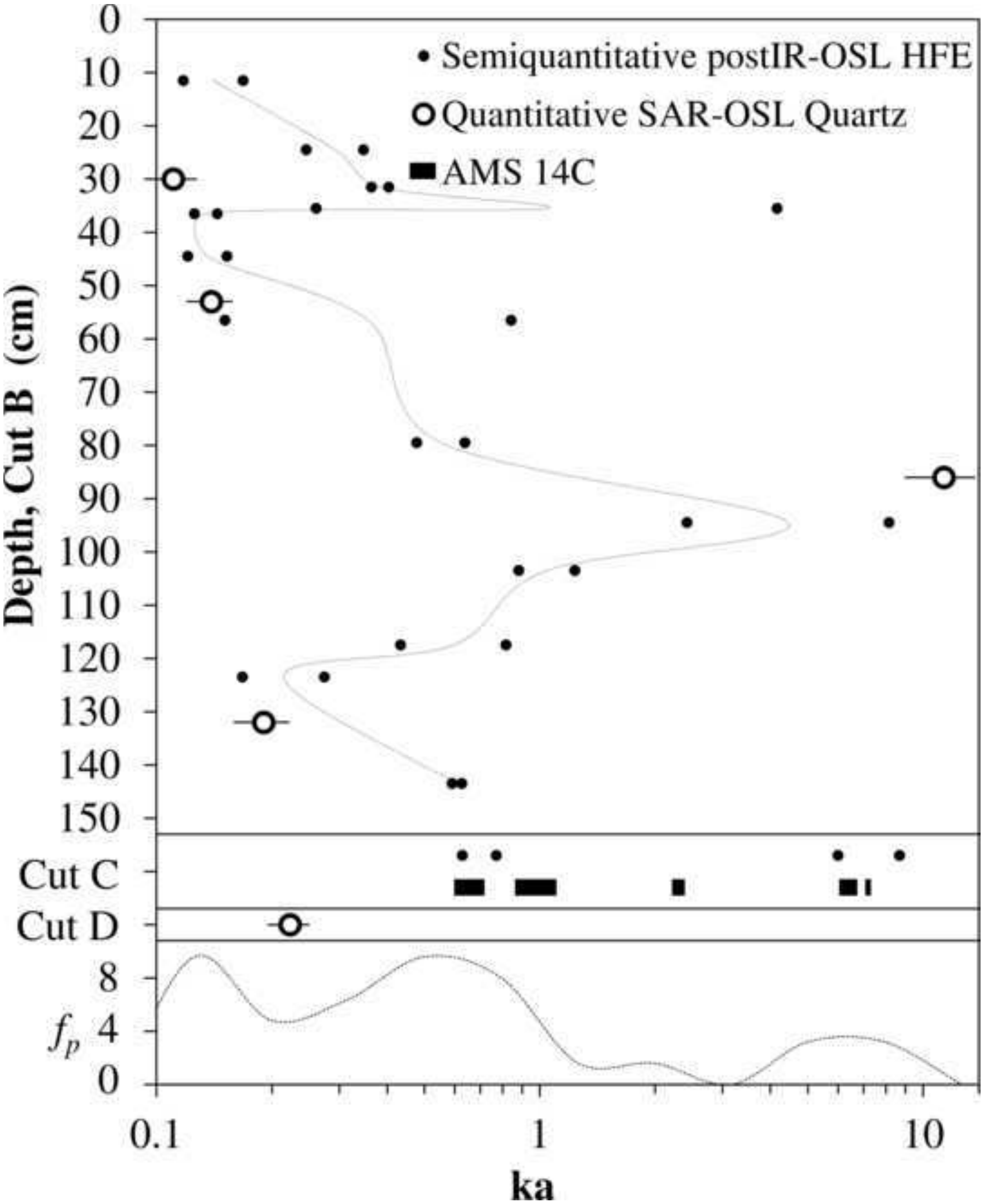

Figure6

Click here to download Figure: Fig.6.eps

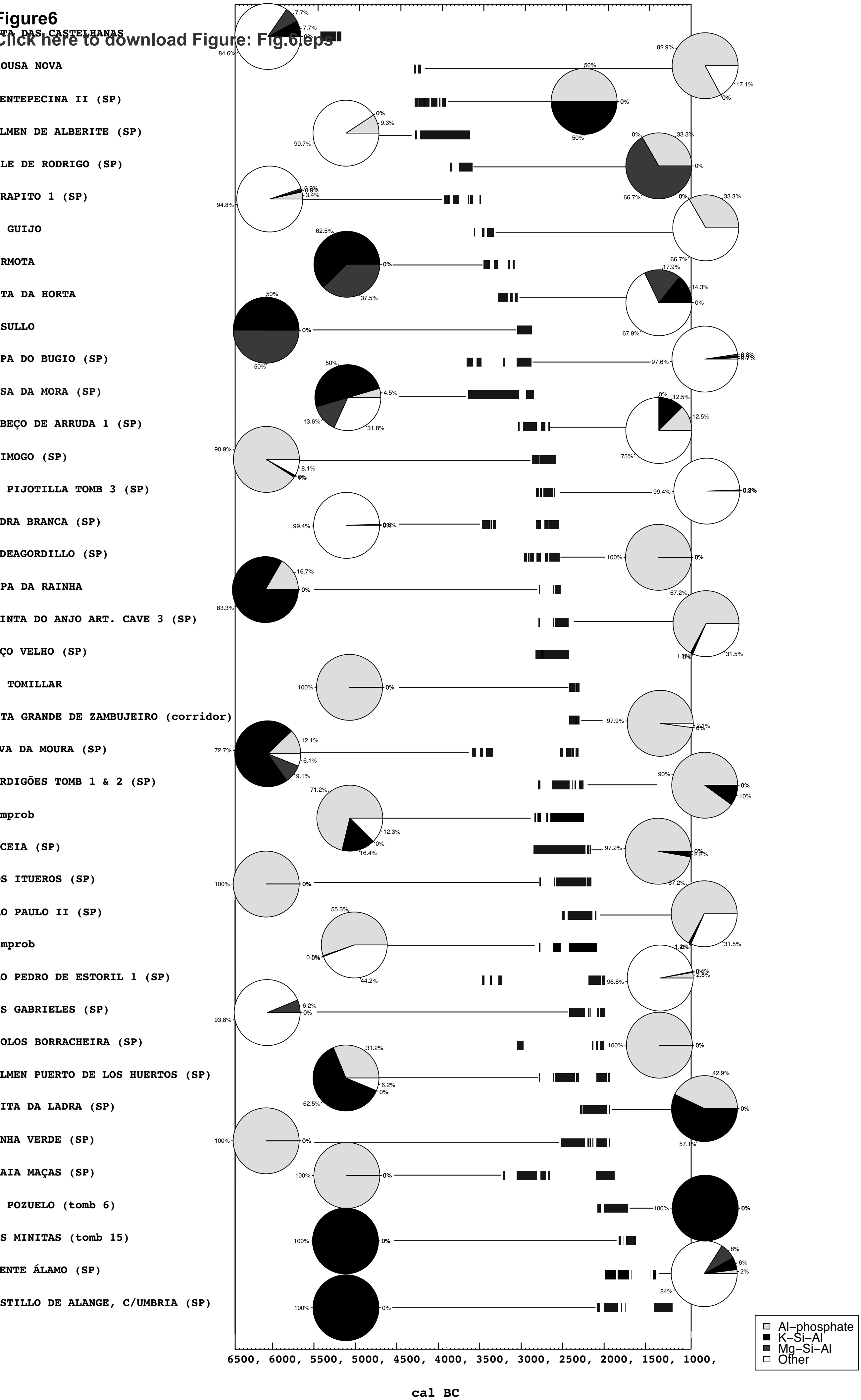

Figure7

Click here to download Figure: Fig.7.eps

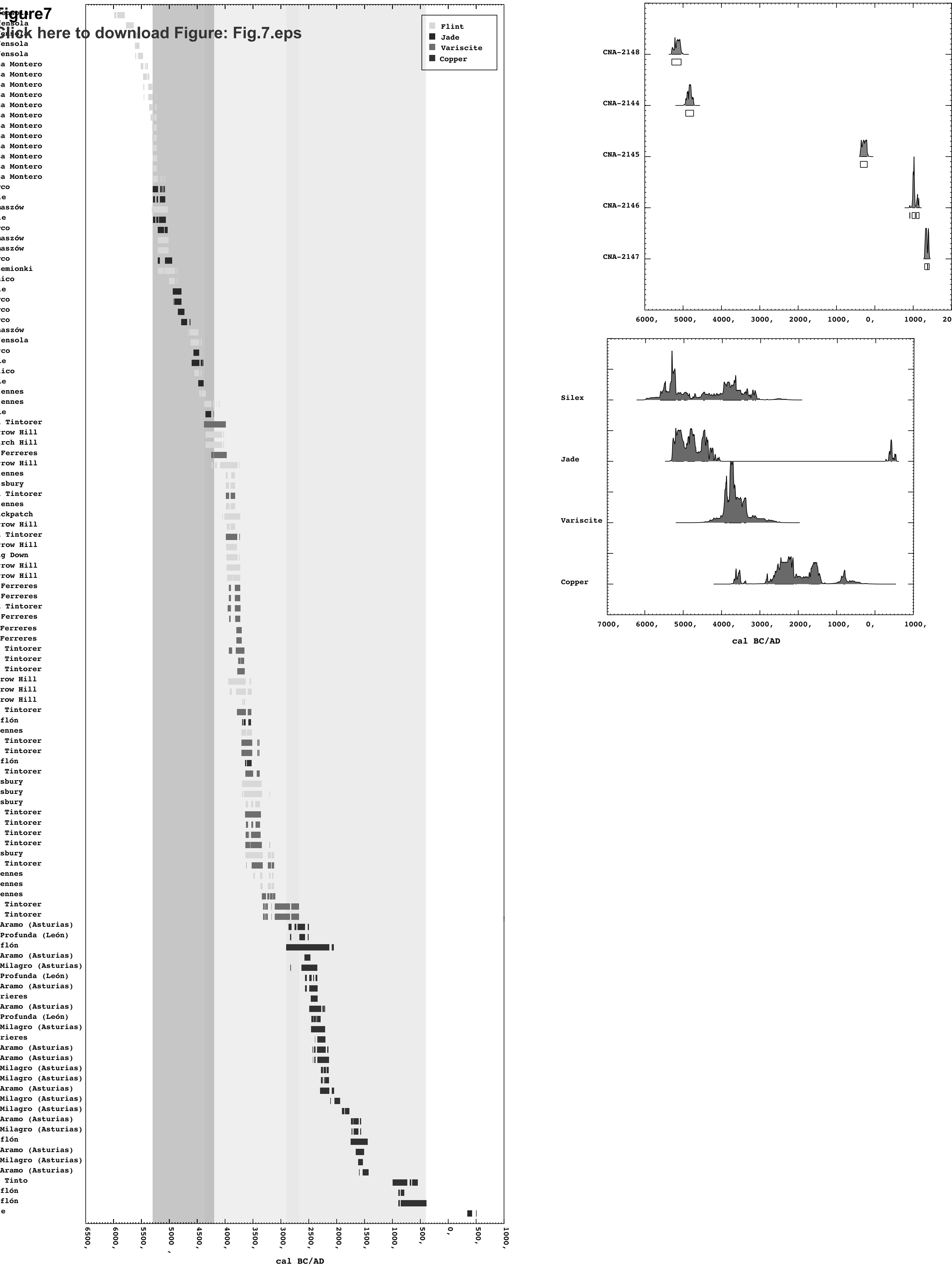

Table1

Table 1. Brief description of the OSL dating sampled units.

Sample #	Cut	Unit	Description
ITNLUM 696	B	6	A bonfire nearby the extraction surface.
ITNLUM 697	B	10	Rock sample. This unit seems to be directly related with the last episode of prehistoric exploitation. This unit accounts for the 15% of the stone tools recovered. Units is cut by the pit
ITNLUM 698	B	13	It is interpreted as a modern depositional unit filling the pit.
ITNLUM 699	B	18	Take part of the oblique depositional units that fills the pit with big rock blocks.
ITNLUM 701	D	6	Depositional unit, believed to be part of production debris accumulation.

Table2

Table 2a: Luminescence dating measurements: radionuclide concentrations and water content estimates.

PCMII	ITNLUM	Sample Type[1]	Depth[2] (cm)	FGS *in situ*[3] K (%)	Th (ppm)	U	H_2O *in situ* (g/g)	HRGS *lab, dry* Ref. A10/	K (%)	Th (ppm)	U	INAA *lab, dry* K (%)	Th (ppm)	U	H_2O *time averaged* (g/g)
1	696	T	30	1.5	9.1	7.6	0.37	256	2.4	13	16	2.2	12	14	0.10
2	697	T	53	1.7	9.6	7.9	0.36	257	2.3	14	15	2.3	12	14	0.19
3	698	R	86	1.5	8.7	7.6	0.37	258	1.8	11	13	1.9	11	11	0.19
4	699	T	132	1.8	7.3	14	0.38	259	2.6	14	23	2.6	12	23	0.20
5	701	T	47	1.7	11	8.1	0.08	260	1.8	12	14	1.7	12	13	0.09
Average uncertainty				*0.1*	*1.2*	*1.1*	*0.02*		*0.1*	*1.8*	*0.6*	*0.2*	*0.7*	*0.4*	*0.15*

[1] Tube; Rock. [2] Below pre-excavation ground level. [3] As measured, i.e. not corrected for in situ water content.

Table 2b: Luminescence dating measurements: summary dose rate, dose, and calendar date estimates.

PCMII	ITNLUM	Sample Type[1]	Depth[2] (cm)	Dose Rate $\dot{D}_{Cosmic}$ (mGy a^{-1})	$\sigma_{\dot{D}}$	$\dot{D}_{total}$ (mGy a^{-1})	$\sigma_{\dot{D}}$	=/</>/?[3]	OSL Reader	Aliquots /24	$\bar{I}_{T1}$[4] (cts)	Absorbed Dose D (Gy ^{60}Co)	σ_D	=/</>/?[3]	Calendar Date *Date*	σ_{date}	
1	696	T	30	0.14	0.04	5.60	0.29	=	2	16	420	0.63	0.09	=	1900	20	AD
2	697	T	53	0.13	0.04	5.25	0.38	=	2	16	215	0.73	0.09	=	1870	20	AD
3	698	R	86	0.12	0.03	4.79	0.31	=	1	22	186	55	11	?	9000	2000	BC
4	699	T	132	0.12	0.03	6.97	0.59	=	3	16	362	1.34	0.19	>	1820	30	AD
5	701	T	47	0.22	0.01	4.79	0.27	=	3	16	2380	1.08	0.12	>	1790	30	AD

[1] Tube; Rock. [2] Below pre-excavation ground level. [3] Summary assessment of dosimetry and luminescence results. =/</> : equal to/overestimates/underestimates "true" value, within quoted uncertainties. ? : potentially outwith uncertainties. [4]Signal Intensity measured in response to the first Test dose in the SAR measurement sequence, averaged over all aliquots.

Table3

Table 3. Results of AMS-radiocarbon dating and anthracological analysis of sampled charcoals from PCM2.

Lab. Code	Specie	Sample	Context	Cut	Unit	Radiocarbon date	Calibrated date (2 σιγμα)
CNA-2144	-	Charcoal	PCM2	C	12	5950±40	4033-4727 BC
CNA-2145	angiosperma	Charcoal	PCM2	C	12/13	2215±35	375-198 BC
CNA-2146	Cf. Cistus sp.	Charcoal	PCM2	C	12	1010±35	910-1152 AD
CNA-2147	Cf. Cistus sp., Cf. Pistacia lentiscus	Charcoal	PCM2	C	12	585±35	1298-1417 AD
CNA-2148	Cf. Quercus suber	Charcoal	PCM2	C	13	6205±40	5295-5051 BC

*According to the calibration curves IntCal13 (samples of the terrestrial biosphere) of Reimer et al. (2013), and using CALIB rev 7.1(Stuiver and Reimer, 1993) program

Table4

Table 4. Results of AMS-radiocarbon dating and anthracological analysis of sampled charcoals from PCM2.

Lab. Code	Specie	Sample	Context	Cut	Unit	14C yr BP	cal yr (2 σ)
CNA-2144	-	Charcoal	PCM2	C	12	5950±40	4933-4727 cal BC
CNA-2145	angiosperma	Charcoal	PCM2	C	12/13	2215±35	379-198 cal BC
CNA-2146	Cf. Cistus sp.	Charcoal	PCM2	C	12	1010±35	969-1152 cal AD
CNA-2147	Cf. Cistus sp., Cf. Pistacia lentiscus	Charcoal	PCM2	C	12	585±35	1298-1417 cal AD
CNA-2148	Cf. Quercus suber	Charcoal	PCM2	C	13	6205±40	5295-5051 cal BC

*According to the calibration curves IntCal13 (samples of the terrestrial biosphere) of Reimer et al. (2013), and using CALIB rev 7.1(Stuiver and Reimer, 1993) program

Table5

Table 5. European mining resources available radiocarbon dates

Lab. code	Site	14C Age	14C Age	d13C	Mineral	Reference
		years BP	years SD	per mil		
Can Tintorer	I-12730	4310	150	0	variscita	(Bosch and Estrada, 1994)
Can Tintorer	I-12731	5350	190	0	variscita	(Bosch and Estrada, 1994)
Can Tintorer	I-11786	5070	100	0	variscita	(Bosch and Estrada, 1994)
Can Tintorer	UBAR-41	4970	100	0	variscita	(Bosch and Estrada, 1994)
Can Tintorer	CSIC-488	4710	50	0	variscita	(Bosch and Estrada, 1994)
Can Tintorer	CSIC-489	4940	50	0	variscita	(Bosch and Estrada, 1994)
Can Tintorer	I-12158	4880	100	0	variscita	(Bosch and Estrada, 1994)
Can Tintorer	UBAR-42	4820	100	0	variscita	(Bosch and Estrada, 1994)
Can Tintorer	I-13099	4820	100	0	variscita	(Bosch and Estrada, 1994)
Can Tintorer	UBAR-49	4740	90	0	variscita	(Bosch and Estrada, 1994)
Can Tintorer	UBAR-30	4710	130	0	variscita	(Bosch and Estrada, 1994)
Can Tintorer	UBAR-48	4690	100	0	variscita	(Bosch and Estrada, 1994)
Can Tintorer	UBAR-47	4610	90	0	variscita	(Bosch and Estrada, 1994)
Can Tintorer	I-12730	4310	150	0	variscita	(Bosch and Estrada, 1994)
Can Tintorer	Beta-61491	4660	110	0	variscita	(Bosch and Estrada, 1994)
Can Tintorer	Beta-72551	4930	70	0	variscita	(Bosch and Estrada, 1994)
Can Tintorer	Beta-72552	5000	60	0	variscita	(Bosch and Estrada, 1994)
Can Tintorer	Beta-72553	5100	60	0	variscita	(Bosch and Estrada, 1994)
S. Ferreres	Beta-155686	5220	110	0	variscita	(Borrell et al., 2009)
S. Ferreres	Beta-250402	5000	40	0	variscita	(Borrell et al., 2009)
S. Ferreres	Beta-250403	4980	40	0	variscita	(Borrell et al., 2009)
S. Ferreres	Beta-250405	4980	40	0	variscita	(Borrell et al., 2009)
S. Ferreres	Beta-250406	5010	40	0	variscita	(Borrell et al., 2009)
S. Ferreres	Beta-250404	5010	40	0	variscita	(Borrell et al., 2009)

Casa Montero	Beta-206512	6410	40	-24.2	silex	(Díaz del Rio and Consuegra Rodríguez, 2011)
Casa Montero	Beta-206513	6270	40	-26.2	silex	(Díaz del Rio and Consuegra Rodríguez, 2011)
Casa Montero	Beta-232884	6360	40	-25.4	silex	(Díaz del Rio and Consuegra Rodríguez, 2011)
Casa Montero	Beta-232885	6280	40	-24.9	silex	(Díaz del Rio and Consuegra Rodríguez, 2011)
Casa Montero	Beta-232886	6350	40	-25.6	silex	(Díaz del Rio and Consuegra Rodríguez, 2011)
Casa Montero	Beta-232887	6290	40	-22.2	silex	(Díaz del Rio and Consuegra Rodríguez, 2011)
Casa Montero	Beta-232888	6240	40	0	silex	(Díaz del Rio and Consuegra Rodríguez, 2011)
Casa Montero	Beta-232889	6290	40	-22.3	silex	(Díaz del Rio and Consuegra Rodríguez, 2011)
Casa Montero	Beta-232890	6500	40	-25.6	silex	(Díaz del Rio and Consuegra Rodríguez, 2011)
Casa Montero	Beta-232891	6320	40	-26.2	silex	(Díaz del Rio and Consuegra Rodríguez, 2011)
Casa Montero	Beta-232892	6270	40	-26.2	silex	(Díaz del Rio and Consuegra Rodríguez, 2011)
Casa Montero	Beta-232893	6330	40	-25.6	silex	(Díaz del Rio and Consuegra Rodríguez, 2011)
Defensola	UTC-1342	6990	80	0	Sílex	(Díaz del Rio et al., 2008)
Defensola	Beta-71143	6820	80	0	Sílex	(Díaz del Rio et al., 2008)
Defensola	Beta-71144	5670	70	0	Sílex	(Díaz del Rio et al., 2008)
Defensola	Beta-80604	6630	70	0	Sílex	(Díaz del Rio et al., 2008)
Defensola	Beta-80603	6540	60	0	Sílex	(Díaz del Rio et al., 2008)
Defensola	UTC-1411	6630	40	0	Sílex	(Díaz del Rio et al., 2008)
Tomaszów	GrN-7594	6145	70	0	Sílex	(Díaz del Rio et al., 2008)
Krzemionki	Gd-1425	6090	110	0	Sílex	(Díaz del Rio et al., 2008)
Porco	AA-62119	5665	47	0	jadeita	(Petrequin et al., 2006)
Porco	AA-62120	5847	47	0	jadeita	(Petrequin et al., 2006)
Porco	AA-62121	6110	48	0	jadeita	(Petrequin et al., 2006)
Porco	AA-62123	5959	49	0	jadeita	(Petrequin et al., 2006)
Porco	AA-62122	6146	49	0	jadeita	(Petrequin et al., 2006)
Porco	AA-62125	5931	48	0	jadeita	(Petrequin et al., 2006)
Porco	AA-62124	6231	48	0	jadeita	(Petrequin et al., 2006)
Bule	AA-66511	1644	36	0	jadeita	(Petrequin et al., 2006)

Bule	AA-66512	5393	42	0	jadeita	(Petrequin et al., 2006)
Bule	AA-66513	5605	42	0	jadeita	(Petrequin et al., 2006)
Bule	AA-66514	5662	71	0	jadeita	(Petrequin et al., 2006)
Bule	AA-66515	6222	44	0	jadeita	(Petrequin et al., 2006)
Bule	AA-66516	5963	61	0	jadeita	(Petrequin et al., 2006)
Bule	AA-66517	6212	71	0	jadeita	(Petrequin et al., 2006)
Cabrieres	Beta-156929	3830	40	0	cobre	(Ambert, 2002)
Cabrieres	Beta-156928	3900	40	0	cobre	(Ambert, 2002)
Araico	Beta-312351	5640	40	0	Silex	(Tarriño et al., 2011)
Araico	Beta-312352	6050	40	0	Silex	(Tarriño et al., 2011)
Tomaszów		6220	120	0	Silex	(Tarriño et al., 2011)
Tomaszów		6145	70	0	Silex	(Tarriño et al., 2011)
Tomaszów		5700	70	0	Silex	(Tarriño et al., 2011)
Blackpatch	BM-290	5090	130	0	silex	(Tarriño et al., 2011)
Church Hill	BM-181	5340	150	0	silex	(Whittle et al., 2011)
Cissbury	BM-183	4720	150	0	silex	(Whittle et al., 2011)
Cissbury	BM-184	4650	150	0	silex	(Whittle et al., 2011)
Cissbury	BM-185	4730	150	0	silex	(Whittle et al., 2011)
Cissbury	BM-3082	5100	60	-19.2	silex	(Whittle et al., 2011)
Cissbury	BM-3086	4710	60	-22.1	silex	(Whittle et al., 2011)
Harrow Hill	BM-182	4930	150	0	silex	(Whittle et al., 2011)
Harrow Hill	BM-2099R	5040	120	-23.1	silex	(Whittle et al., 2011)
Harrow Hill	BM-2097R	5140	150	-25.2	silex	(Whittle et al., 2011)
Harrow Hill	BM-2071R	4900	120	-26.7	silex	(Whittle et al., 2011)
Harrow Hill	BM-2075R	5020	110	-26.4	silex	(Whittle et al., 2011)
Harrow Hill	BM-2124R	5060	90	-24.9	silex	(Whittle et al., 2011)
Harrow Hill	BM-2098R	5350	150	-25.7	silex	(Whittle et al., 2011)
Harrow Hill	BM-3084	4880	30	-21.9	silex	(Whittle et al., 2011)

Harrow Hill	BM-3085	5070	50	-23.4	silex	(Whittle et al., 2011)
Long Down	OxA-1152	5050	100	0	silex	(Whittle et al., 2011)
Spiennes	Lv-1566	5510	55	0	silex	(Whittle et al., 2011)
Spiennes	GrN-4674	5420	75	0	silex	(Collet, 2004; 2008)
Spiennes	Lv-1598	5100	65	0	silex	(Collet, 2004; 2008)
Spiennes	KN-I.16	5110	40	0	silex	(Collet, 2004; 2008)
Spiennes	OxA-3196	4830	80	0	silex	(Collet, 2004; 2008)
Spiennes	Beta-194770	4580	40	0	silex	(Collet, 2004; 2008)
Spiennes	Beta-194771	4550	40	0	silex	(Collet, 2004; 2008)
Spiennes	Beta-110683	4500	50	0	silex	(Collet, 2004; 2008)
El Milagro (Asturias)	OxA-3005	3990	90	0	cobre	(Collet, 2004; 2008)
El Milagro (Asturias)	OxA-3006	3850	90	0	cobre	(Blas Cortina, 2011)
El Milagro (Asturias)	Ua-33207	3785	35	0	cobre	(Blas Cortina, 2011)
El Milagro (Asturias)	Ua-33209	3775	35	0	cobre	(Blas Cortina, 2011)
El Milagro (Asturias)	Ua-24538	3630	40	0	cobre	(Blas Cortina, 2011)
El Milagro (Asturias)	Ua-24537	3520	40	0	cobre	(Blas Cortina, 2011)
El Milagro (Asturias)	Ua-24550	3355	45	0	cobre	(Blas Cortina, 2011)
El Milagro (Asturias)	Ua-33206	3285	35	0	cobre	(Blas Cortina, 2011)
La Profunda (León)	Ua-35778	3865	35	0	cobre	(Blas Cortina, 2011)
La Profunda (León)	Ua-35779	3950	35	0	cobre	(Blas Cortina, 2011)
La Profunda (León)	Ua-35780	4075	35	0	cobre	(Blas Cortina, 2011)
El Aramo (Asturias)	OxA-1833	4090	70	0	cobre	(Blas Cortina, 2011)
El Aramo (Asturias)	OxA-1926	3810	70	0	cobre	(Blas Cortina, 2011)
El Aramo (Asturias)	OxA-3007	3900	90	0	cobre	(Blas Cortina, 2011)
El Aramo (Asturias)	OxA-6789	3995	50	0	cobre	(Blas Cortina, 2011)
El Aramo (Asturias)	Ua-18629	3775	65	-21.4	cobre	(Blas Cortina, 2011)
El Aramo (Asturias)	Ua-18630	3365	60	-20.1	cobre	(Blas Cortina, 2011)
El Aramo (Asturias)	Ua-18631	3310	65	-20.4	cobre	(Blas Cortina, 2011)

El Aramo (Asturias)	Ua-18632	3825	60	-20.5	cobre	(Blas Cortina, 2011)
El Aramo (Asturias)	Ua-18633	3940	60	-20.1	cobre	(Blas Cortina, 2011)
El Aramo (Asturias)	Ua-18634	3215	55	-22	cobre	(Blas Cortina, 2011)
Chiflón	BM-1600	4840	50	0	cobre	(Blas Cortina, 2011)
Chiflón	BM-1599	4780	50	0	cobre	(Acosta, 1995)
Chiflón	OxTL-200e3(II)	4000	300	0	cobre	(Acosta, 1995)
Rio Tinto	BM-2337R	2650	140	0	cobre	(Acosta, 1995)
Chiflón	BM-1529	3320	130	0	cobre	(Castro Martínez et al., 1996)
Chiflón	BM-1528	2650	60	0	cobre	(Burleigh et al., 1982)
Chiflón	BM-1601	2520	210		cobre	(Burleigh et al., 1982; Rothenberg and Frejeiro, 1980)

Table6

Table 6: Studied sites available radiocarbon dates

Lab. code	*Site*	*14C Age*	*14C Age*	*d13C*	*Reference*
		years BP	years SD	per mil	
Beta-83084	ALDEAGORDILLO	4320	70	0	(Fabián García, 2006)
GrN-19168	ALDEAGORDILLO	4115	20	0	(Fabián García, 2006)
Beta-83085	ALDEAGORDILLO	4100	80	0	(Fabián García, 2006)
Beta-194313	ANTA DA HORTA	4480	40	-19.7	(Oliveira, 2010)
ICEN-1264	ANTA DAS CASTELHANAS	6360	110	0	(Oliveira, 2000)
Beta-243693	ANTA GRANDE DE ZAMBUJEIRO (corridor)	3910	40	0	(Soares and SIlva, 2010)
Beta-123363	CABEÇO DA ARRUDA I	4370	70	0	(Waterman, 2012)
Beta-132975	CABEÇO DA ARRUDA I	4240	50	0	(Waterman, 2012)
GrN-5110	CARAPITO 1	4850	40	0	(Senna-Martínez and Quintã Ventura, 2000)
OxA-3733	CARAPITO 1	5125	70	0	(Senna-Martínez and Quintã Ventura, 2000)
TO-3336	CARAPITO 1	5120	40	0	(Senna-Martínez and Quintã Ventura, 2000)
OxA-5506	CASA DA MOURA	4600	90	0	(Cardoso et al., 1996)
TO-953	CASA DA MOURA	5990	60	-19.6	(Cardoso et al., 1996)
TO-2092	CASA DA MOURA	4850	100	-19.3	(Cardoso et al., 1996)
TO-2093	CASA DA MOURA	5070	70	-19.2	(Cardoso et al., 1996)
TO-2094	CASA DA MOURA	5020	70	-19.6	(Cardoso et al., 1996)
ICEN-802	CASA DA MOURA (1A)	6100	70	0	(Cardoso et al., 1996)
Beta-68667	CASTILLO DE ALANGE (c/ Umbria 3/ N. II)	3080	90	0	(Pavón Soldevila, 1994)
CNA-346	CASULLO	4410	50	0	(Linares Catela and García Sanjuán, 2010)
Beta-277240	CHOUSA NOVA	5450	40	0	(Dominguez Bella and Bóveda, 2011)
UBAR-593	COVA DA MOURA	4715	50	0	(Silva, 2003)
UBAR-536	COVA DA MOURA	3950	60	0	(Silva, 2003)
ICEN-1040	DOLMEN DA PEDRA BRANCA (chamber)	4620	60	-19.7	(Soares, 2010)
ICEN-1041	DOLMEN DA PEDRA BRANCA (corridor)	4120	60	-20.06	(Soares, 2010)
Beta-80602	DOLMEN DE ALBERITE	5320	70	0	(Sttip and Tamers, 1996)
Beta-80600	DOLMEN DE ALBERITE	5110	140	0	(Sttip and Tamers, 1996)
Beta-80598	DOLMEN DE ALBERITE	5020	70	0	(Sttip and Tamers, 1996)
Poz-55021	EL GUIJO	4695	35	0	(Villalobos García, 2014)
Teledyne 19080	EL POZUELO (tomb 6)	3580	120	0	(Linares Catela and García Sanjuán, 2010)
GrN-18875	EL TOMILLAR	3925	40	0	(Fabián García, 2006)
GrN-18669	FUENTEPECINA II	5375	45	0	(Delibes de Castro and Rojo Guerra, 1997)
GrN-16073	FUENTEPECINA II	5170	100	0	(Delibes de Castro and Rojo Guerra, 1997)

Beta-176899	HERDADE DOS CEBOLINHOS (ANTA 2/ chamber)	3900	40	0	(Gonçalves, 2003)
Beta-177471	HERDADE DOS CEBOLINHOS (ANTA 2)	3840	40	0	(Gonçalves, 2003)
Beta-121143	LA PIJOTILLA (T3 UE 15)	4130	40	0	(Odriozola et al., 2008)
ITN A6/209	LA PIJOTILLA (T3/ layer 16/ vessel 15)	2716	96	0	(Odriozola et al., 2008)
CNA-034	LA PIJOTILLA (T3/ layer 18)	4168	55	0	(Odriozola et al., 2008)
UGAMS 8455	LAPA DA RAINHA	4080	25	0	(Waterman, 2012)
GrN-5628	LAPA DO BUGIO	4850	45	0	(Silva and Wasterlain, 2010)
OxA-5507	LAPA DO BUGIO	4420	110	0	(Silva and Wasterlain, 2010)
Beta-142035	LAS MINITAS (tomb 15)	3430	50	0	(Pavón Soldevila, 1994)
ICEN-674	LECEIA	4370	60	0	(Cardoso, 2014)
Wk-34424	LECEIA	3833	26	0	(Cardoso, 2014)
ICEN-95	LECEIA (C2)	4370	60	1.34	(Cardoso, 2014)
ICEN-89	LECEIA (C2)	4200	70	- 19.91	(Cardoso, 2014)
ICEN-92	LECEIA (C2)	4120	80	- 24.56	(Cardoso, 2014)
ICEN-102	LECEIA (C2)	3970	70	1.68	(Cardoso, 2014)
ICEN-1217	LECEIA (C2)	4020	80	- 22.64	(Cardoso, 2014)
ICEN-1220	LECEIA (C2)	4030	70	- 20.05	(Cardoso, 2014)
ICEN-737	LECEIA (C2)	3920	70	- 19.56	(Cardoso, 2014)
ICEN-315	LECEIA (C2)	3730	170	- 21.19	(Cardoso, 2014)
ICEN-1213	LECEIA (C2)	3970	70	- 23.21	(Cardoso, 2014)
ICEN-1218	LECEIA (C2)	3910	60	- 23.27	(Cardoso, 2014)
ICEN-1211	LECEIA (C2)	3900	80	- 25.05	(Cardoso, 2014)
ICEN-1215	LECEIA (C2)	3900	70	-20.9	(Cardoso, 2014)
ICEN-1216	LECEIA (C2)	3880	80	- 21.22	(Cardoso, 2014)
ICEN-1214	LECEIA (C2)	3840	110	- 26.21	(Cardoso, 2014)
ICEN-314	LECEIA (C2)	3770	130	- 25.75	(Cardoso, 2014)
ICEN-91	LECEIA (C3)	4130	60	-20	(Cardoso, 2014)
ICEN-673	LECEIA (C3)	4130	100	-24.9	(Cardoso, 2014)

ICEN-675	LECEIA (C3)	4100	90	-25.4	(Cardoso, 2014)
ICEN-1173	LECEIA (C3)	4170	50	-20.5	(Cardoso, 2014)
ICEN-1175	LECEIA (C3)	4090	80	-19.85	(Cardoso, 2014)
ICEN-1176	LECEIA (C3)	4090	60	-20.02	(Cardoso, 2014)
ICEN-1177	LECEIA (C3)	4050	50	-21.12	(Cardoso, 2014)
LY-4205	LECEIA (C3)	4030	120	-21.2	(Cardoso, 2014)
ICEN-1160	LECEIA (C4)	4630	60	0	(Cardoso, 2014)
ICEN-312	LECEIA (C4)	4530	100	0	(Cardoso, 2014)
ICEN-316	LECEIA (C4)	4520	70	0	(Cardoso, 2014)
ICEN-312	LECEIA (C4)	4530	100	-20.22	(Cardoso, 2014)
ICEN-313	LECEIA (C4)	4520	130	-22	(Cardoso, 2014)
ICEN-316	LECEIA (C4)	4520	70	-22.02	(Cardoso, 2014)
ICEN-1275	LECEIA (EN)	3950	90	0	(Cardoso, 2014)
ICEN-1241	LECEIA (EN)	3950	90	0	(Cardoso, 2014)
Beta-260295	LECEIA (EN)	3840	40	0	(Cardoso, 2014)
Beta-260296	LECEIA (EN)	3980	40	0	(Cardoso, 2014)
Sac-1317	LECEIA (FM)	4220	50	0	(Cardoso, 2014)
Sac-1317	LECEIA (FM)	4220	50	0	(Cardoso, 2014)
Beta-260297	LECEIA (FM)	4140	40	0	(Cardoso, 2014)
Beta-260299	LECEIA (FM)	4100	40	0	(Cardoso, 2014)
Sac-1317	LECEIA (FM)	4220	40	0	(Cardoso, 2014)
Beta-260297	LECEIA (FM)	4140	40	0	(Cardoso, 2014)
Beta-260299	LECEIA (FM)	4100	40	0	(Cardoso, 2014)
ICEN-1160	LECEIA (layer 4)	4630	45	-21.81	(Cardoso, 2014)
ICEN-1161	LECEIA (layer 4)	4440	50	-23.39	(Cardoso, 2014)
ICEN-1159	LECEIA (layer 4)	4430	50	-21.35	(Cardoso, 2014)
ICEN-1158	LECEIA (layer 4)	4320	50	-21.45	(Cardoso, 2014)
Beta-185650	LOS GABRIELES (dolmen 4/ chamber 2)	3700	50	0	(Linares Catela and García Sanjuán, 2010)
Beta-185648	LOS GABRIELES (dolmen 4/ chamber 3)	3850	40	0	(Linares Catela and García Sanjuán, 2010)
Beta-185649	LOS GABRIELES (dolmen 4/ chamber 4)	3920	50	0	(Linares Catela and García Sanjuán, 2010)
I-16150	LOS ITUEROS	4120	130	0	(Fabián García, 2006)
I-83088	LOS ITUEROS	3960	90	0	(Fabián García, 2006)

I-16149	LOS ITUEROS	3850	100	0	(Fabián García, 2006)
OxA-5535	MARMOTA 2	4600	55	0	(Gonçalves, 2002)
Sac-2122	MOITA DA LADRA	3700	50	0	(Cardoso and Caninas, 2010)
Sac-2123	MOITA DA LADRA	3700	50	0	(Cardoso and Caninas, 2010)
Sac-2370	MOITA DA LADRA	3930	80	0	(Cardoso and Caninas, 2010)
Sac-2371	MOITA DA LADRA	3810	60	0	(Cardoso and Caninas, 2010)
ICEN-957	OLIVAL DA PEGA 2B (phase VF1/OP4)	4130	60	0	(Gonçalves, 2002)
ICEN-956	OLIVAL DA PEGA 2B (phase VF3/OP2)	4180	80	0	(Gonçalves, 2002)
ICEN-955	OLIVAL DA PEGA 2B (phase VF3/OP3)	4290	100	0	(Gonçalves, 2002)
Sac-1556	PAIMOGO	4259	90	0	(Gonçalves, 2002)
UBAR-539	PAIMOGO	4139	90	0	(Gonçalves, 2002)
Beta-186854	PENEDO DE LEXIM (locus 1/ layer 19)	4080	50	-20.5	(Sousa, 2010)
Beta-142451	PENEDO DE LEXIM (locus 1/ layer 19)	3820	40	0	(Sousa, 2010)
Sac-2067	PENEDO DE LEXIM (locus 1/ layer 19)	3820	50	- 20.74	(Sousa, 2010)
Sac-2156	PENEDO DE LEXIM (locus 1	layer 9)	3640	0	(Sousa, 2010)
Beta-186855	PENEDO DE LEXIM (locus 3/ layer 19)	3760	40	-19.6	(Sousa, 2010)
Beta-175775	PENEDO DE LEXIM (locus 3b/ layer 10)	4080	40	-21.2	(Sousa, 2010)
Sac-2158	PENEDO DE LEXIM (locus 3b/ layer 7)	3880	60	0	(Sousa, 2010)
Sac-2069	PENEDO DE LEXIM (locus 3b/ layer 7b)	3930	30	-21.2	(Sousa, 2010)
Sac-2168	PENEDO DE LEXIM (locus 5/ layer 8)	3760	50	0	(Sousa, 2010)
Beta-175774	PENEDO DE LEXIM (locus3b/ layer 16)	4100	40	-20.2	(Sousa, 2010)
W-656	PENHA VERDE	3420	200	0	(Cardoso, 2010)
W-656	PENHA VERDE	3420	200	0	(Cardoso, 2010)
Beta-260300	PENHA VERDE (22/064)	4000	40	0	(Cardoso, 2010)
Beta-276400	PENHA VERDE (ditch HUT 2)	3970	40	0	(Cardoso, 2010)
Beta-276399	PENHA VERDE (HUT 1)	3890	40	0	(Cardoso, 2010)
Beta-296578	PENHA VERDE (HUT 2)	3700	30	0	(Cardoso, 2010)
Beta-296580	PENHA VERDE (HUT 3)	3680	40	0	(Cardoso, 2010)
Beta-276398	PENHA VERDE (pavement HUT 2)	3830	40	0	(Cardoso, 2010)
Beta-327750	PERDIGÕES (Tomb 1)	4030	40	0	(Valera et al., 2014)
Beta-327748	PERDIGÕES (Tomb 1)	4060	30	0	(Valera et al., 2014)
Beta-327747	PERDIGÕES (Tomb 1)	4130	30	0	(Valera et al., 2014)
Beta-308789	PERDIGÕES (Tomb 2)	3840	30	0	(Valera et al., 2014)
Beta-308791	PERDIGÕES (Tomb 2)	4090	30	0	(Valera et al., 2014)
Beta-308792	PERDIGÕES (Tomb 2)	3890	30	0	(Valera et al., 2014)
Beta-308793	PERDIGÕES (Tomb 2)	3970	30	0	(Valera et al., 2014)
OxA-5533	POÇO VELHO	4245	55	0	(Gonc□alves, 2008)
OxA-5532	POÇO VELHO	4090	55	0	(Gonc□alves, 2008)
Beta-244396	POÇO VELHO (F-2)	4090	40	-19.1	(Gonc□alves, 2008)

Beta-245137	POÇO VELHO (F-2)	4030	40	-10.2	(Gonc□alves, 2008)
Beta-244397	POÇO VELHO (F-2)	3920	40	-19.8	(Gonc□alves, 2008)
Beta-244394	POÇO VELHO (F-3)	4520	40	-19.1	(Gonc□alves, 2008)
Beta-245138	POÇO VELHO (F-3)	4500	40	-19.1	(Gonc□alves, 2008)
Beta-244395	POÇO VELHO (F-3)	4030	40	-18.5	(Gonc□alves, 2008)
OxA-5533	POÇO VELHO (SIF)	4245	55	-19.4	(Gonc□alves, 2008)
Beta-244393	POÇO VELHO (SIF)	4160	50	-19.1	(Gonc□alves, 2008)
Beta-178464	POÇO VELHO (SIF)	4150	40	-19.3	(Gonc□alves, 2008)
Beta-244390	POÇO VELHO (SIF)	4150	40	0	(Gonc□alves, 2008)
OxA-5532	POÇO VELHO (SIF)	4090	55	-19.6	(Gonc□alves, 2008)
Beta-244392	POÇO VELHO (SIF)	3970	40	-18.8	(Gonc□alves, 2008)
Beta-178463	POÇO VELHO (SIF)	3960	40	-19.7	(Gonc□alves, 2008)
Beta-244391	POÇO VELHO (SIF)	48090	1200	-20.1	(Gonc□alves, 2008)
H-2049/148	PRAIA DAS MAÇAS (chamber)	4260	60	0	(Gonçalves, 2002)
H-2048/1458	PRAIA DAS MAÇAS (chamber)	3650	60	0	(Gonçalves, 2002)
OxA-5509	PRAIA DAS MAÇAS (west chamber)	4410	75	0	(Gonçalves, 2002)
OxA-5510	PRAIA DAS MAÇAS (west chamber)	4395	60	0	(Gonçalves, 2002)
Leisner & Frreira/ 1963	PRAIA DAS MAÇAS (west chamber)	4160	110	0	(Gonçalves, 2002)
Leisner & Frreira/ 1963	PRAIA DAS MAÇAS (west chamber)	3650	100	0	(Gonçalves, 2002)
CNA-342	PUERTO DE LOS HUERTOS	4070	50	0	(Linares Catela and García Sanjuán, 2010)
CNA-344	PUERTO DE LOS HUERTOS	3940	50	0	(Linares Catela and García Sanjuán, 2010)
CNA-341	PUERTO DE LOS HUERTOS	3680	50	0	(Linares Catela and García Sanjuán, 2010)
GrN-10744	QUINTA DO ANJO (H-3)	4040	70	0	(Gonçalves, 2002)
OxA-5508	QUINTA DO ANJO (H-3)	4050	60	0	(Gonçalves, 2002)
UBAR-629	S. PAULO II	3960	190	0	(Silva, 2003)
UBAR-630	S. PAULO II	3870	70	0	(Silva, 2003)
Beta-188390	S. PEDRO DE ESTORIL 1	4720	40	-19	(Gonçalves, 2005)
Beta-178467	S. PEDRO DE ESTORIL 1	3830	40	-19.4	(Gonçalves, 2005)
Beta-178468	S. PEDRO DE ESTORIL 1	3790	40	-19.6	(Gonçalves, 2005)
UGAMS 8455	THOLOS DA BORRACHEIRA	4420	25	0	(Waterman, 2012)
UGAMS 8454	THOLOS DA BORRACHEIRA	3720	25	0	(Waterman, 2012)
Ua-10831	VALE DE RODRIGO (chamber)	3905	75	0	(Boaventura, 2011)
Ua-10830	VALE DE RODRIGO (chamber)	4905	60	0	(Boaventura, 2011)
KIA-31381	VALE DE RODRIGO 3 (layer 8)	4996	29	0	(Boaventura, 2011)
KIA-27559	ZAMBUJAL (ant. Phase 1)	4238	29	0	(Kunst and Lutz, 2011)
KIA-7260	ZAMBUJAL (ant. Phase 1a)	4134	43	0	(Kunst and Lutz, 2011)
KIA-27563	ZAMBUJAL (ant. phase 3b)	4065	37	0	(Kunst and Lutz, 2011)
KIA-28669	ZAMBUJAL (ant. Phase 4)	4001	28	0	(Kunst and Lutz, 2011)
KIA-27557	ZAMBUJAL (ant. Phase 4)	3996	23	0	(Kunst and Lutz, 2011)

KIA-27558	ZAMBUJAL (phase 1)	4129	31	0	(Kunst and Lutz, 2011)
KIA-7259	ZAMBUJAL (phase 1a)	3801	43	0	(Kunst and Lutz, 2011)
KIA-7258	ZAMBUJAL (phase 1a)	3891	43	0	(Kunst and Lutz, 2011)
KIA-4509	ZAMBUJAL (phase 1a)	3960	44	0	(Kunst and Lutz, 2011)
KIA-7256	ZAMBUJAL (phase 1b)	3951	55	0	(Kunst and Lutz, 2011)
GrN-7009	ZAMBUJAL (phase 1c)	4200	40	0	(Kunst and Lutz, 2011)
KIA-7257	ZAMBUJAL (phase 1c)	3836	39	0	(Kunst and Lutz, 2011)
GrN-6671	ZAMBUJAL (phase 2)	4170	55	0	(Kunst and Lutz, 2011)
GrN-7002	ZAMBUJAL (phase 2)	4050	40	0	(Kunst and Lutz, 2011)
KIA-27561	ZAMBUJAL (phase 2)	4155	32	0	(Kunst and Lutz, 2011)
KIA-27562	ZAMBUJAL (phase 2)	4049	25	0	(Kunst and Lutz, 2011)
KN-4989	ZAMBUJAL (phase 2)	3917	50	0	(Kunst and Lutz, 2011)
KN-4990	ZAMBUJAL (phase 2)	3934	51	0	(Kunst and Lutz, 2011)
KN-4988	ZAMBUJAL (phase 2)	3980	40	0	(Kunst and Lutz, 2011)
KIA-7261	ZAMBUJAL (phase 2b/c)	3842	37	0	(Kunst and Lutz, 2011)
KIA-27564	ZAMBUJAL (phase 3)	3992	32	0	(Kunst and Lutz, 2011)
KN-I.115	ZAMBUJAL (phase 3/4)	3530	65	0	(Kunst and Lutz, 2011)
GrN-7003	ZAMBUJAL (phase 3b)	4055	40	0	(Kunst and Lutz, 2011)
GrN-7004	ZAMBUJAL (phase 3b)	3995	35	0	(Kunst and Lutz, 2011)
GrN-7005	ZAMBUJAL (phase 3c)	4055	40	0	(Kunst and Lutz, 2011)
GrN-7008	ZAMBUJAL (phase 3c)	3980	35	0	(Kunst and Lutz, 2011)
GrN-6670	ZAMBUJAL (phase 3c/4a)	4150	105	0	(Kunst and Lutz, 2011)
KIA-28668	ZAMBUJAL (phase 4)	3999	29	0	(Kunst and Lutz, 2011)
GrN-7006	ZAMBUJAL (phase 4a/c)	4090	40	0	(Kunst and Lutz, 2011)
GrN-6669	ZAMBUJAL (phase 4b)	4025	95	0	(Kunst and Lutz, 2011)
GrN-7007C	ZAMBUJAL (phase 4b)	3950	65	0	(Kunst and Lutz, 2011)
GrN-6668	ZAMBUJAL (phase 4c/d)	3625	65	0	(Kunst and Lutz, 2011)
KN-4507	ZAMBUJAL (phase 5)	3466	53	0	(Kunst and Lutz, 2011)
KN-4506	ZAMBUJAL (phase 5)	3847	34	0	(Kunst and Lutz, 2011)
KIA-27565	ZAMBUJAL (post. phase 3b)	4445	31	0	(Kunst and Lutz, 2011)
KIA-27556	ZAMBUJAL (post. phase 3b)	3965	32	0	(Kunst and Lutz, 2011)
KIA-27566	ZAMBUJAL (post. Phase 5)	3467	36	0	(Kunst and Lutz, 2011)
KIA-27641	ZAMBUJAL (post. Phase 5)	2381	40	0	(Kunst and Lutz, 2011)

Video
Click here to download Video: video.mp4